
The following resources related to this article are available online at <http://stke.sciencemag.org>.
This information is current as of 3 May 2011.

- Article Tools** Visit the online version of this article to access the personalization and article tools:
<http://stke.sciencemag.org/cgi/content/full/sigtrans;3/151/rs3>
- Supplemental Materials** "Supplementary Materials"
<http://stke.sciencemag.org/cgi/content/full/sigtrans;3/151/rs3/DC1>
- Related Content** The editors suggest related resources on *Science's* sites:
<http://stke.sciencemag.org/cgi/content/abstract/sigtrans;4/154/eg1>
<http://stke.sciencemag.org/cgi/content/abstract/sigtrans;3/137/eg6>
<http://stke.sciencemag.org/cgi/content/abstract/sigtrans;3/124/ra44>
<http://stke.sciencemag.org/cgi/content/abstract/sigtrans;3/104/ra3>
- References** This article has been **cited by** 4 article(s) hosted by HighWire Press; see:
<http://stke.sciencemag.org/cgi/content/full/sigtrans;3/151/rs3#BIBL>
This article cites 131 articles, 49 of which can be accessed for free:
<http://stke.sciencemag.org/cgi/content/full/sigtrans;3/151/rs3#otherarticles>
- Glossary** Look up definitions for abbreviations and terms found in this article:
<http://stke.sciencemag.org/glossary/>
- Permissions** Obtain information about reproducing this article:
<http://www.sciencemag.org/about/permissions.dtl>

ATM-Dependent and -Independent Dynamics of the Nuclear Phosphoproteome After DNA Damage

Ariel Bensimon,^{1*†} Alexander Schmidt,^{2,3*} Yael Ziv,¹ Ran Elkon,⁴ Shih-Ya Wang,⁵ David J. Chen,⁵ Ruedi Aebersold,^{2,6,7‡} Yosef Shiloh^{1‡}

(Published 7 December 2010; Volume 3 Issue 151 rs3)

The double-strand break (DSB) is a cytotoxic DNA lesion caused by oxygen radicals, ionizing radiation, and radiomimetic chemicals. Cells cope with DNA damage by activating the DNA damage response (DDR), which leads either to damage repair and cellular survival or to programmed cell death. The main transducer of the DSB response is the nuclear protein kinase ataxia telangiectasia mutated (ATM). We applied label-free quantitative mass spectrometry to follow the dynamics of DSB-induced phosphoproteome in nuclear fractions of the human melanoma G361 cells after radiomimetic treatment. We found that these dynamics are complex, including both phosphorylation and dephosphorylation events. In addition to identifying previously unknown ATM-dependent phosphorylation and dephosphorylation events, we found that about 40% of DSB-induced phosphorylations were ATM-independent and that several other kinases are potentially involved. Sustained activity of ATM was required to maintain many ATM-dependent phosphorylations. We identified an ATM-dependent phosphorylation site on ATM itself that played a role in its retention on damaged chromatin. By connecting many of the phosphorylated and dephosphorylated proteins into functional networks, we highlight putative cross talks between proteins pertaining to several cellular biological processes. Our study expands the DDR phosphorylation landscape and identifies previously unknown ATM-dependent and -independent branches. It reveals insights into the breadth and complexity of the cellular responses involved in the coordination of many DDR pathways, which is in line with the critical importance of genomic stability in maintenance of cellular homeostasis.

INTRODUCTION

DNA damage is a major threat to genomic stability and consequently to cellular homeostasis. Cells respond to DNA damage by activating the DNA damage response (DDR), a complex process that includes DNA repair mechanisms, chromatin reorganization, cell cycle checkpoints, modulation of gene expression, and many signaling pathways (1). An often cytotoxic DNA lesion is the double-strand break (DSB), which is induced by ionizing radiation, oxygen radicals, and radiomimetic chemicals. DSBs activate a particularly vigorous DDR and are therefore commonly used to explore its complexity (2, 3).

The DSB response is initiated by a heterogeneous group of proteins commonly termed “sensors” that are rapidly recruited to the damaged

sites where they are involved in initial damage processing and local chromatin reorganization. The sensors also set the scene for the activation of the transducers—protein kinases that spread the DNA damage alarm by phosphorylating numerous effectors in various DDR branches (4, 5). The chief transducer of the DSB response is ATM (ataxia telangiectasia mutated), a kinase that is rapidly activated after DSB induction and that phosphorylates a plethora of downstream substrates, many of which are key proteins in processes affected by the DDR (3, 6).

Mutations that lead to ATM loss or inactivation cause a severe genomic instability syndrome, ataxia telangiectasia (A-T) (7, 8). ATM belongs to a family of phosphatidylinositol 3-kinase-like protein kinases (PIKKs) that also includes two other DDR transducers: ATR (ATM and Rad3-related) (9) and DNA-dependent protein kinase (DNA-PK) (10). The preferred targets of the three kinases are serine or threonine residues followed by glutamines (SQ or TQ). ATR responds primarily to stalled replication forks, whereas DNA-PK is a key player in DSB repair mediated by nonhomologous end-joining. The three kinases are functionally related, and ATR is thought to phosphorylate a number of ATM substrates in response to DSBs, albeit at later time points after the occurrence of DSBs and with a lower efficiency relative to ATM (9, 11, 12).

Different types of posttranslational modifications, such as phosphorylation, ubiquitination, SUMOylation, and acetylation, are induced in response to DSBs and are involved in the rapid dissemination of the DSB alarm (13–16). Among these, protein phosphorylation is a prevalent posttranslational modification; therefore, exploration of DSB-induced phosphoproteome dynamics should reveal insights into the breadth and complexity of this cellular response and identify previously unknown branches of the DDR. Previous large-scale studies were aimed at identifying direct PIKK

¹David and Inez Myers Laboratory for Cancer Genetics, Department of Human Molecular Genetics and Biochemistry, Sackler School of Medicine, Tel Aviv University, Tel Aviv 69978, Israel. ²Institute of Molecular Systems Biology, Eidgenössische Technische Hochschule Zurich, Zurich 8093, Switzerland. ³Biozentrum, University of Basel, Basel 4056, Switzerland. ⁴Division of Gene Regulation, Netherlands Cancer Institute, Plesmanlaan 121, 1066 CX, Amsterdam, Netherlands. ⁵Division of Molecular Radiation Biology, Department of Radiation Oncology, University of Texas Southwestern Medical Center, Dallas, TX 75390-9187, USA. ⁶Competence Center for Systems Physiology and Metabolic Diseases, Eidgenössische Technische Hochschule Zurich, Zurich 8093, Switzerland. ⁷Faculty of Science, University of Zurich, Zurich 8057, Switzerland.

*These authors contributed equally to this work.

†Present address: Institute of Molecular Systems Biology, Eidgenössische Technische Hochschule Zurich, Zurich 8093, Switzerland.

‡To whom correspondence should be addressed. E-mail: yossih@post.tau.ac.il (Y.S.); rudolf.aebersold@imsb.biol.ethz.ch (R.A.)

targets by immunoprecipitation and mass spectrometric analysis of proteins containing pSQ or pTQ sites (13, 17). The unbiased isolation of phosphopeptides followed by their analysis using quantitative liquid chromatography–mass spectrometry (LC-MS) (18–21) provides a more general approach to explore DSB-induced phosphoproteome dynamics. This type of analysis has been used for the exploration of the cellular phosphoproteome after various stimuli (22–26). This strategy also detects dephosphorylation, a regulatory event that may be as important as phosphorylation, but that has not been extensively documented in the DDR.

We conducted label-free quantitative phosphoproteomic analyses after the induction of DSBs in the presence or absence of an ATM inhibitor to distinguish between ATM-dependent and -independent changes in the phosphoproteome in enriched nuclear fractions. The results expand our knowledge of the molecular networks that constitute the cellular response to DNA damage and reveal previously unknown characteristics of this essential process.

RESULTS

Modulation of the nuclear phosphoproteome after DNA damage

To identify damage-induced alterations in the nuclear phosphoproteome of cultured human cells, we implemented a quantitative phosphoproteomics strategy that combined selective phosphopeptide enrichment and label-free quantification based on LC-MS (fig. S1A). We used the G361 human melanoma cell line in which there is abundant endogenous, active ATM (27). In two independent experiments, cells were treated with the radiomimetic drug neocarzinostatin (NCS) (200 ng/ml) and harvested after 10, 30, 120, and 360 min (table S1). Extracts were prepared from a crude nuclear fraction obtained by one-step hypotonic enrichment (Fig. 1A). Isolation, detection, identification, and quantification of phosphopeptides were performed as described in Materials and Methods. ATM activation and activity were monitored, respectively, by following ATM's damage-induced autophosphorylation on Ser¹⁹⁸¹ (28) and the phosphorylation of the ATM substrate, KAP1 [KRAB (Krueppel-associated box)-associated protein-1], on Ser⁸²⁴ (29) (Fig. 1B).

We identified a total of 3073 phosphopeptides, which mapped to 2871 phosphorylation sites on 1099 proteins (tables S13 and S14). Using the annotation tool DAVID (30), we found that 574 of these proteins had been previously annotated in SwissProt as located to the nucleus; this represented a significant nuclear enrichment [$P < 5 \times 10^{-112}$, after false discovery rate (FDR) correction for multiple testing]. The distributions of the individual residues phosphorylated (Ser/Thr/Tyr) and the number of phosphoryl groups per peptide were similar to those obtained in previous studies (Fig. 1C) (18, 19). We quantified the changes in the abundance of phosphopeptides between samples by calculating the average \log_2 ratios between NCS-treated and untreated samples. Seeking phosphorylation sites that were modulated in response to DSBs, we applied filtering criteria based on signal-to-noise evaluation (fig. S1, B and C). We considered phosphopeptides as damage-responsive phosphorylation events (phosphorylation and loss of phosphorylation were regarded equally) if they showed more than a fourfold change in abundance in at least two consecutive time points after NCS treatment, comparing NCS-treated to untreated samples, with an estimated FDR of 7%. We identified 753 phosphorylation sites mapping to 394 proteins that were modulated in response to NCS treatment in the time course experiment. Of these phosphorylation sites, 411 represented damage-induced phosphorylations and 342 represented loss of phosphorylation (Fig. 1D and table S2), which we attributed primarily to phosphorylation and dephosphorylation events, respectively. It

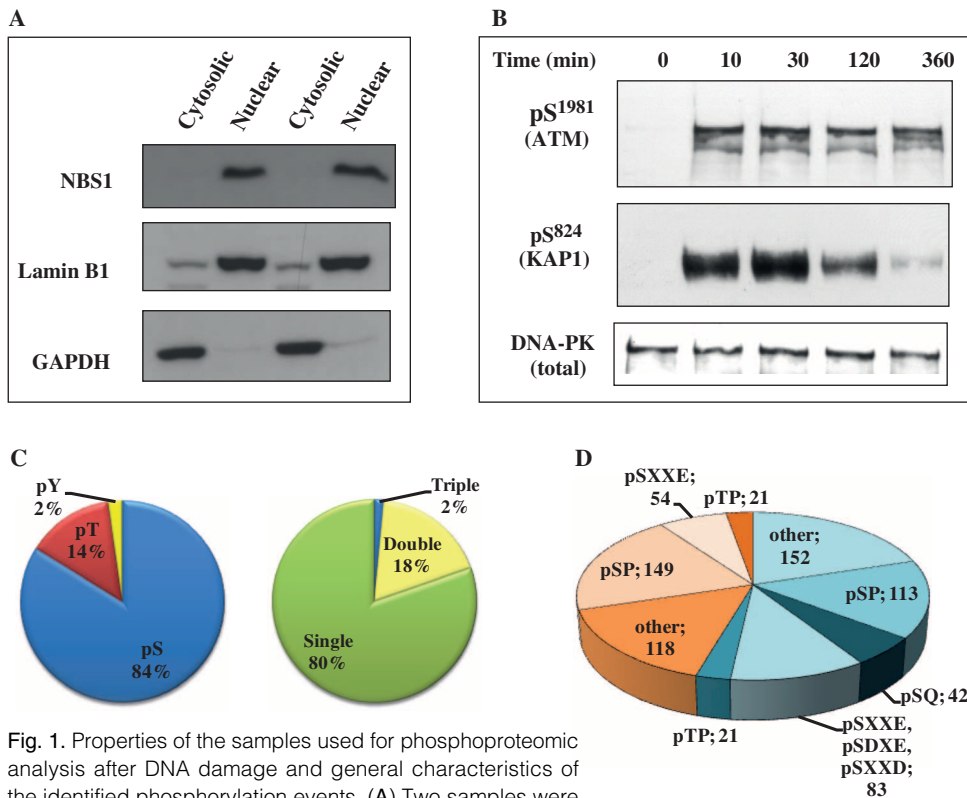


Fig. 1. Properties of the samples used for phosphoproteomic analysis after DNA damage and general characteristics of the identified phosphorylation events. **(A)** Two samples were enriched for nuclear fractions with a one-step hypotonic fractionation. Enrichment was assessed by Western blotting of the cytoplasmic marker GAPDH, which indicated that only residual amounts of this protein remained in the nuclear-enriched fraction. Lamin B1 and NBS1 were used as markers for nuclear proteins. **(B)** Activation of ATM and the DDR was verified by monitoring the autophosphorylation of ATM on Ser¹⁹⁸¹ and the ATM-dependent phosphorylation of the KAP1 protein on Ser⁸²⁴ performed by Western blotting analysis of nuclear extracts. The catalytic subunit of DNA-PK served as a loading control. Samples were collected at indicated times after administration of NCS (200 ng/ml). **(C)** General properties of the identified phosphoproteome. Left: The distribution of individually identified sites according to the residue that was phosphorylated demonstrated that tyrosine phosphorylation occurred on less than 3% of phosphorylation sites. Right: The distribution of the number of phosphoryl groups per peptide indicated that more than 80% of peptides identified had a single phosphorylation. **(D)** Pie chart distribution of DSB-responsive phosphorylation (blue) and dephosphorylation (orange) events subdivided according to overrepresented motifs identified using Motif-X.

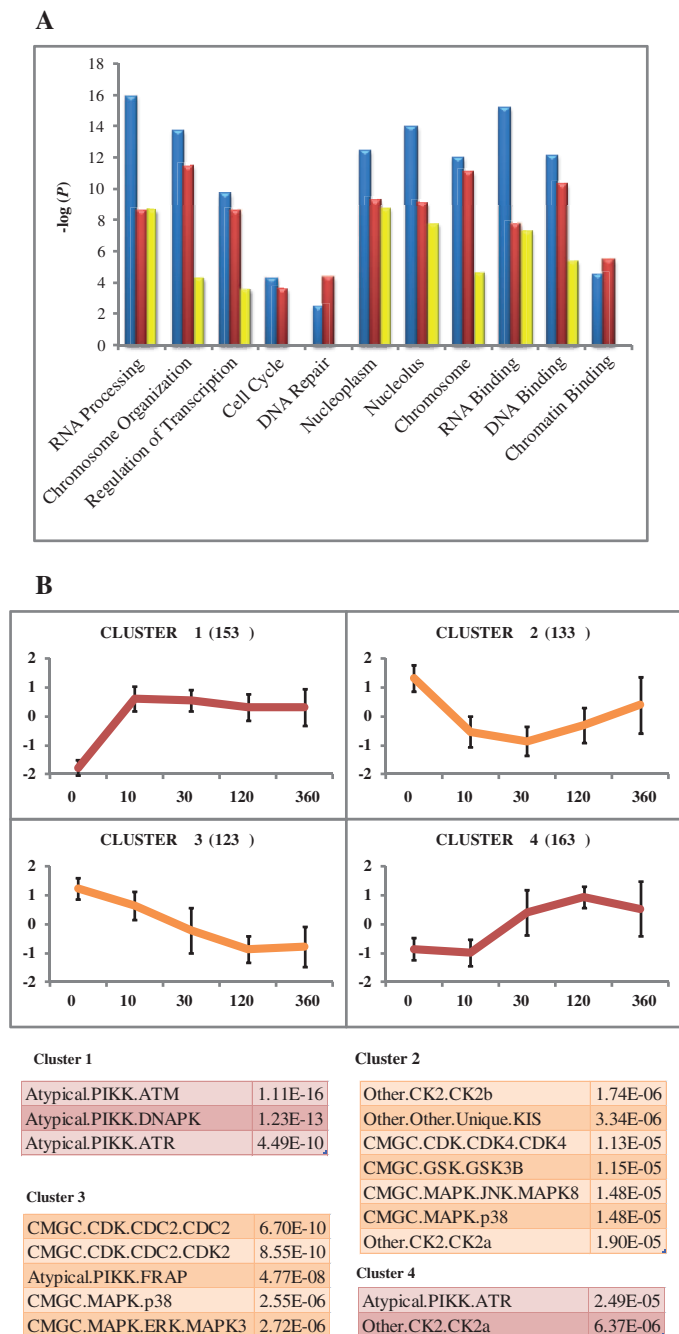


Fig. 2. Properties of the DNA damage–responsive phosphoproteome. (A) Enriched GO terms associated with all proteins that exhibited a change in phosphorylation state in response to DNA damage (blue), phosphorylated proteins (red), and dephosphorylated proteins (yellow). The y axis represents the $-\log_{10}$ of the P value after FDR correction for multiple testing. (B) Kinetic patterns of the individual phosphorylation sites. Four patterns were identified by clustering analysis with the CLICK algorithm. Upper graphs show the time courses of the clusters. The x axis represents the time points (in minutes). The y axis represents \log_2 -based ratios for each phosphorylation site standardized to mean 0 and SD 1. In parentheses is the number of phosphorylation sites in each cluster. Lower lists show selected enriched kinase predictions with the lowest P values for each cluster.

is possible that some of these changes in the abundance of the phosphopeptides could reflect other processes, such as changes in the protein amounts or in the subcellular localization after the DNA damage. Additionally, changes in phosphorylation may be masked by changes in other posttranslational modifications occurring on the same peptide, which may be detected as an apparent change in phosphorylation.

To analyze the amino acid composition surrounding the identified phosphorylation sites, we used Motif-X (31) to search for overrepresented motifs (fig. S2A). Although we found the motif pSQ in the group of sites that increased in phosphorylation, as expected (Fig. 1D), this motif comprised a relatively small fraction (~10%) of the detected damage-responsive phosphorylation sites, suggesting that the damage-induced phosphorylation arena is considerably wider than PIKK-mediated phosphorylations. Other overrepresented motifs were pSP, pSXXE, and pTP, which were identified in both damage-induced phosphorylation sites and sites where phosphorylation was reduced (Fig. 1D and fig. S2A).

Although only in-depth analysis will reveal the importance or relevance of each of the phosphorylation and dephosphorylation events that we identified in the DDR, several of the sites that we identified have been reported in other studies, providing evidence that the data set is valid. The phosphorylated sites that we identified included 10 ATM-mediated phosphorylations that had been previously studied in detail: ATM Ser¹⁸⁹³ (32), ATM Ser¹⁹⁸¹ (28), KAP1 Ser⁸²⁴ (29), NBS1 Ser³⁴³ (33), RAD50 Ser⁶³⁵ (34), SMC1 Ser⁹⁵⁷ (35), SMC3 Ser¹⁰⁶⁷, Ser¹⁰⁸³ (36), and TP53BP1 Ser⁸³¹, Ser¹²¹⁹ (37, 38). In addition, 30 phosphorylation sites of SQ or TQ motifs that were recorded in a previous proteomic screen for ATM or ATR targets (13) appeared in our list of damage-induced phosphorylations. Although we and Matsuoka *et al.* (13) both identified a total of 102 proteins, in only 21 proteins were the same phosphorylation site identified in both studies. Different phosphorylation sites on the same protein may play specific roles in modulating its functions after DNA damage (39).

We performed an initial functional analysis of the acquired and lost phosphorylations (analyzed separately or together) by searching for significantly overrepresented Gene Ontology (GO) terms with the GO tool in DAVID (30). Most of the identified processes and functions were related to nucleic acid metabolism or chromatin organization (Fig. 2A and table S3), with predominance of “Chromosome Organization” and “RNA Processing” and their daughter terms. The group of proteins with increased phosphorylation showed a more significant enrichment of almost all of the identified biological processes and molecular functions relative to those enriched in the group of proteins with decreased phosphorylation (table S3). The exceptions were “RNA Splicing” and “Spliceosome,” which were more significantly enriched in the group of proteins showing decreased phosphorylation.

The cellular response to DSBs, particularly the early phase, is believed to be mediated primarily by ATM-dependent protein phosphorylation. Because most phosphorylation events that we found to be increased in response to DNA damage did not occur on the typical PIKK target motif, S/TQ, we searched the phospho.ELM (version 8.2) (40) and PhosphoSitePlus (41) databases for kinases documented to phosphorylate proteins from our lists on the phosphorylation sites found in our data set. About 75% of the phosphorylation sites that changed in response to DNA damage were included in at least one of these databases (fig. S2B). However, only 6% were matched to a known kinase (table S4). Among these kinases were ATM, cell division control 2 homolog [CDC2, also known as cyclin-dependent kinase 1 (CDK1)], CDK2, and casein kinase 2 (CK2). To expand the list of putative kinases involved in the observed increases in phosphorylation, we predicted putative kinase target sites with the GPS 2.1 software (42). We statistically substantiated this analysis

by adding enrichment tests to detect predicted kinase targets that were overrepresented among our damage-responsive increased phosphorylation events. We associated the enriched kinase predictions with overrepresented sequence motifs identified by Motif-X to draw putative links between these two analyses. We found the expected enrichment for targets of the PIKKs ATM, ATR, and DNA-PK, linked to the pSQ motif as expected, and we also observed a significant enrichment for targets of CK1, CK2, GRK2 [G protein (heterotrimeric guanosine triphosphate-binding protein)-coupled receptor kinase 2], and KIS (serine-threonine protein kinase Kist) linked to the pSXXE/D motif (Table 1 and table S5). KIS was the only enriched kinase linked to the pSP motif among the increased phosphorylation events. Using kinase prediction enrichment analysis, we noted enrichment for targets of CDKs, MAPKs (mitogen-activated protein kinases), FRAP (FKBP-12 rapamycin-associated protein), GSK3B (glycogen synthase kinase 3β), and PLK1 (Polo-like kinase 1) in the sites that exhibited a decrease in phosphorylation in response to DNA damage, suggesting that sites phosphorylated by these kinases might be dephosphorylated after DNA damage (Table 1 and table S5). These enriched kinase dephosphorylated targets could be linked to the pSP motif, found by Motif-X.

Using DAVID for annotation, we generated GO-annotated subsets of phosphorylated and dephosphorylated proteins to gain insight into the functions of the kinases associated with targets that exhibited a change in phosphorylation status during DDR (table S6). “Chromosome Organization” proteins were enriched for ATM and CK2 targets, whereas “DNA Repair” proteins were enriched for ATM and DNA-PK targets. CK2 targets were enriched in proteins annotated “Adenyl Ribonucleotide Binding,” suggesting a putative role for this kinase in the regulation of enzymes in response to DNA damage. Among the proteins with reduced phosphorylation, CK2 targets were enriched among “RNA Processing” proteins, and targets of CDC2, CDK2, and JNK (c-Jun N-terminal kinase) were highly enriched in the “Regulation of Transcription” group (table S6). Thus, this analysis validated known relationships between processes and functions associated with the DDR and certain kinases, and suggested previously unknown relationships for kinases within the DDR, such as CK2.

Table 1. Kinase target predictions enriched in the lists of phosphorylated and dephosphorylated sites. Kinase targets were predicted with the GPS software. Enrichment tests used the hypergeometric dis-

Kinetics of the damage-induced modulation of the nuclear phosphoproteome

Using the CLICK clustering algorithm implemented in the microarray analysis suite EXPANDER, we divided the damage-induced changes in phosphorylation events into clusters according to their temporal patterns (43, 44). Manually unifying clusters with similar patterns resulted in four distinct clusters representing the major kinetic responses (Fig. 2B and table S2). The temporal patterns represented by these clusters indicated that some phosphorylation and dephosphorylation events occurred rapidly after DNA damage and peaked within minutes, whereas others developed more slowly. Only clusters with consistent kinetic patterns (which represented 77% of the observed damage-responsive phosphorylation events) were used in this analysis (table S2).

We asked whether specific temporal patterns were enriched for predicted substrates of certain kinases. Using GPS, we found that phosphorylation events that rapidly increased (Fig. 2B, cluster 1) were significantly enriched for targets of ATM, ATR, and DNA-PK, whereas induced events with slower kinetics (Fig. 2B, cluster 4) were enriched for targets of CK2 and ATR (table S7). Phosphorylation events that rapidly decreased after DNA damage (Fig. 2B, cluster 2) were enriched for targets of CK2b and KIS. Phosphorylation events that decreased with slower kinetics (Fig. 2B, cluster 3) were enriched for targets of CDKs, MAPKs, and FRAP. To further explore the temporal patterns, we used DAVID to determine the significant enrichment of GO-associated biological processes and molecular compartments with the proteins in these clusters (table S8). As expected, all of the clustered phosphorylated proteins were significantly associated with the nucleus, but less expected was the substantial variation in the assignments across the temporal patterns, such as the association with the nucleolus and chromosome. Annotations to DNA Repair, Chromatin Binding, and Regulation of Transcription were only associated with the rapidly phosphorylated proteins (cluster 1), whereas proteins related to RNA Processing were associated with all patterns except the slowly dephosphorylated group (cluster 3). In general, more annotations were associated with rapidly occurring phosphorylation changes versus slowly occurring ones, which is consistent with the importance of a rapid response to DNA damage.

tribution. *P* value cutoff for enrichment is set at 5×10^{-5} . The full hierarchy of each kinase is presented. Only individually identified kinases, not kinase families, are shown here. Table S5 contains the complete list.

Phosphorylated sites	<i>P</i> value	Dephosphorylated sites	<i>P</i> value
Atypical.PIKK.ATM	4.84×10^{-14}	CMGC.CDK.CDC2.CDC2	2.81×10^{-12}
Other.CK2.CK2a	7.57×10^{-14}	CMGC.CDK.CDC2.CDK2	6.94×10^{-12}
Atypical.PIKK.ATR	2.28×10^{-11}	CMGC.GSK.GSK3B	7.58×10^{-11}
Atypical.PIKK.DNAPK	5.7×10^{-11}	CMGC.MAPK.ERK.MAPK3	1.8×10^{-10}
Other.Other.Unique.KIS	2.71×10^{-8}	Atypical.PIKK.FRAP	8.8×10^{-10}
Other.CK2.CK2b	2.3×10^{-7}	CMGC.CDK.CDK4.CDK4	8.87×10^{-10}
AGC.GRK.BARK.GRK.2	3.09×10^{-6}	CMGC.MAPK.p38.MAPK14	2.97×10^{-9}
CK1.CK1.CK1a	4.82×10^{-6}	Other.Other.Unique.KIS	3.33×10^{-9}
		CMGC.CDK.CDK5	5.73×10^{-9}
		CMGC.MAPK.ERK.MAPK1	8.98×10^{-9}
		CMGC.MAPK.ERK.MAPK7	9.09×10^{-9}
		CMGC.MAPK.JNK.MAPK10	1.55×10^{-8}
		CMGC.DYRK.Dyrk1	2.52×10^{-8}
		CMGC.MAPK.JNK.MAPK8	4.59×10^{-8}
		AGC.GRK.BARK.GRK.2	8.6×10^{-8}
		Other.PLK.PLK1	2.38×10^{-7}
		CMGC.MAPK.p38.MAPK12	4.23×10^{-7}
		CMGC.MAPK.JNK.MAPK9	3.41×10^{-5}
		Other.CK2.CK2a	3.59×10^{-5}

Network organization of DNA damage-responsive proteins

To put the observed phosphoproteome dynamics in a systems context and obtain putative functional organization of the signaling networks reflected in the data, we interfaced our protein lists with various protein-protein interaction (PPI) networks. Using the STRING database of PPIs (45), we first identified proteins within our lists that were directly interconnected and then processed the interaction network of 161 of our 394 proteins with Cytoscape (46) (fig. S3). Rather than clustering this network to infer protein complexes, we searched the CORUM database (47) for complexes containing at least two proteins from our lists. Through this analysis, 109 of our proteins that exhibited changes in phosphorylation in response to DNA damage were assigned to 100 complexes (table S9). Some of the proteins were members of several complexes, linking them into an extended interaction network. Proteins and complexes pertaining to biological processes, such as RNA Processing, Chromosome Organization, and DNA Repair, were interlaced to a functional network (Fig. 3A and fig. S4). The complex-based analysis revealed that the proteins on our list are members of complexes, such as WINAC (a chromatin remodeling complex), CEN (centromere chromatin complex), CDC5L (involved in RNA splicing), and the Spliceosome, indicating that functions of these complexes may be affected upon DNA damage. Several proteins, such as SMARCC1 (a component of chromatin-remodeling complexes), HNRNPU, and EFTUD2 [both involved in pre-messenger RNA (mRNA) splicing], interacted with several complexes, and thus, the damage-induced modulation of their function may affect several processes at the same time.

To identify key proteins and functional modules, we assumed that certain functional interactions between damage-responsive proteins could be mediated by proteins that do not appear in our lists. The inclusion of these “connecting” proteins in the analysis expanded the interaction networks and assisted in identifying additional functional modules. We used the PPI Spider tool (48), which enabled us to connect 245 proteins from our lists into a network with a total of 386 nodes (fig. S5), in which only one PPI Spider-added intermediate protein was allowed between two proteins from our lists. To ensure that the proteins added to the network by PPI Spider were of functional relevance to the DDR, we compared the effect of this analysis on the significance of GO terms found by DAVID (table S10). Whereas comparison of the GO term enrichment for the 245 connected proteins to the original 394 proteins showed a relatively small effect on GO enrichment, the addition of the 141 connecting proteins by PPI Spider had a marked impact on the significance of some of the GO terms (table S10). For example, the significance of RNA Splicing, DNA Binding, Regulation of Transcription, and daughter terms were increased by more than 10 orders of magnitude.

We used the Cytoscape plug-in CentiScaPe (49) to calculate several topological parameters of the PPI network. The distribution of the number of “edges” (interactions) connected to the “nodes” (proteins) in the network pointed to a scale-free topology (fig. S6A), as has been shown previously for other protein interaction networks (50–52). Most of the nodes in this network had only few edges, whereas a few nodes, termed “hubs,” had more edges than the average and probably represent key players (50, 51, 53). We defined hubs as proteins in the top 5% of the degree distribution, representing nodes with seven or more edges. We identified 18 hubs, of which 15 were from our data set; 14 nodes could be incorporated into an interconnected network with STRING (Fig. 3C). Among these 15 were the DDR-associated protein kinases ATM and DNA-PK; chromatin-binding proteins, such as SMARCA4, SMC1A, SIN3A, and HCFC1; and splicing-associated proteins, such as CD2BP2 and SFRS1. The interconnected hub proteins may represent part of a “core” module involved in DNA damage, chromatin organization, and

RNA processing. At least six of the hub proteins are functionally linked to the DDR, including ATM, DNA-PK, TP53 (54, 55), MYC (56, 57), SMC1A (35), and SMARCA4 (58). Thus, our topological analysis may reveal other proteins in key positions in the DDR.

To search for functional modules in the PPI Spider extended network of 386 nodes, we used the GO tool BiNGO (version 2.3) (59) in Cytoscape. Networks were created for functional modules representing proteins annotated as DNA Repair and Chromosome Organization (Fig. 3B) or as RNA Processing (fig. S6B) by including proteins added by PPI Spider to extend the networks and reveal additional connections and organizational structures. In the DNA Repair and Chromosome Organization network, the addition of proliferating cell nuclear antigen (PCNA) and SMARCA5 allowed connection of several chromatin-related proteins to each other: CBX3, CHAF1A, CHAF1B, and BAZ2A (all of which were phosphorylated); BAZ1A (which was dephosphorylated); and RSF1, BAZ1B, and KAP1 (which were both phosphorylated and dephosphorylated). Both BAZ1B and CHAF1A are members of chromatin remodeling complexes, and these proteins have been shown to have a role in the replication of pericentric heterochromatin (60, 61), to which KAP1 can be recruited (62). Both CHAF1A and BAZ1B interact with PCNA (63–66), which facilitates their recruitment to replication foci. Certain of these proteins have known roles in the DDR: KAP1 is found in the vicinity of heterochromatin during DSB repair (29, 67, 68), and BAZ1B has a role in maintaining H2AX phosphorylation on Ser¹³⁹, a marker of domains flanking DSBs (69). However, a direct functional link between BAZ1B and CHAF1A has not been documented. At the network organization level, our analysis revealed that proteins regulated by both phosphorylation and loss of phosphorylation can be “meshed” into functional modules, stressing the importance of events that reduce phosphorylation (likely dephosphorylation) in the DDR.

ATM dependence of DSB-induced phosphorylation dynamics

In view of our finding that ~90% of damage-responsive phosphorylation events did not occur on the well-documented ATM and ATR S/TQ motif, we examined the degree of ATM dependence of the phosphoproteome dynamics. The ATM inhibitor KU55933 (70) inhibits ATM activity within minutes after its administration into cell culture (71). KU55933 (denoted hereafter ATMi) was added to G361 cultures 30 min before NCS treatment, and its effect on phosphoproteome dynamics was assessed 30 and 120 min after NCS addition and compared with samples treated with NCS only (Fig. 4A). A total of 457 phosphorylation sites mapping to 277 proteins were modulated by more than fourfold at these time points in response to NCS and were evaluated for their ATM dependence (table S11). Using the CLICK clustering algorithm, we grouped phosphorylation events according to their modulation after damage induction in the presence or absence of ATMi (Fig. 4B). We defined a phosphorylation event as ATM-dependent if it was reduced by at least 50% at the log₂ ratio when ATMi was added before NCS treatment. About 60% of damage-responsive phosphorylation and loss of phosphorylation events were ATM-dependent by this criterion (Fig. 4B). Searching for enriched kinase predictions (table S12), we found that, as expected, ATM-dependent sites were enriched for predicted targets of PIKKs, but we also noticed targets of GRKs, nuclear factor κ B-inducing kinase (NIK), and CK2, raising the possibility that after DNA damage these protein kinases are subject to ATM-dependent regulation. A search among ATM-independent phosphorylation sites revealed a significant enrichment for potential KIS targets. Among the ATM-dependent loss of phosphorylation events, predicted targets of KIS, CDC2, and FRAP were enriched, whereas ATM-independent loss of phosphorylation events showed significant overrepresentation of GSK and p38 kinase families.

ATM is rapidly activated in response to DSBs and can be abruptly “switched off” by ATMi (71). This allowed us to examine the effect of ATM inactivation 15 min after damage induction on the damage-induced phosphoproteome dynamics (Fig. 4A, right panel). Application of the CLICK clustering algorithm to these data yielded four clusters (Fig. 4C). We termed phosphorylation events affected by ATM switch off after damage induction as “ATM-regulated” to distinguish them from the larger set of “ATM-dependent” events. Of the 457 phosphorylation sites evaluated, ~50% were ATM-regulated; 65% of the damage-induced phospho-

phorylation events that were ATM-dependent were also ATM-regulated. For example, known ATM-dependent phosphorylation events that are maintained for extended periods of time after damage induction rapidly decayed after ATM switch off 15 min after NCS administration (Fig. 4D). This suggests that maintained phosphorylation at these sites requires sustained ATM activity, possibly due to concomitant counteraction by protein phosphatases or due to protein turnover. Only 33% of ATM-dependent decreased phosphorylation events (Fig. 4B, cluster 3) were also ATM-regulated (Fig. 4C, in cluster 4). This result suggests that ATM may

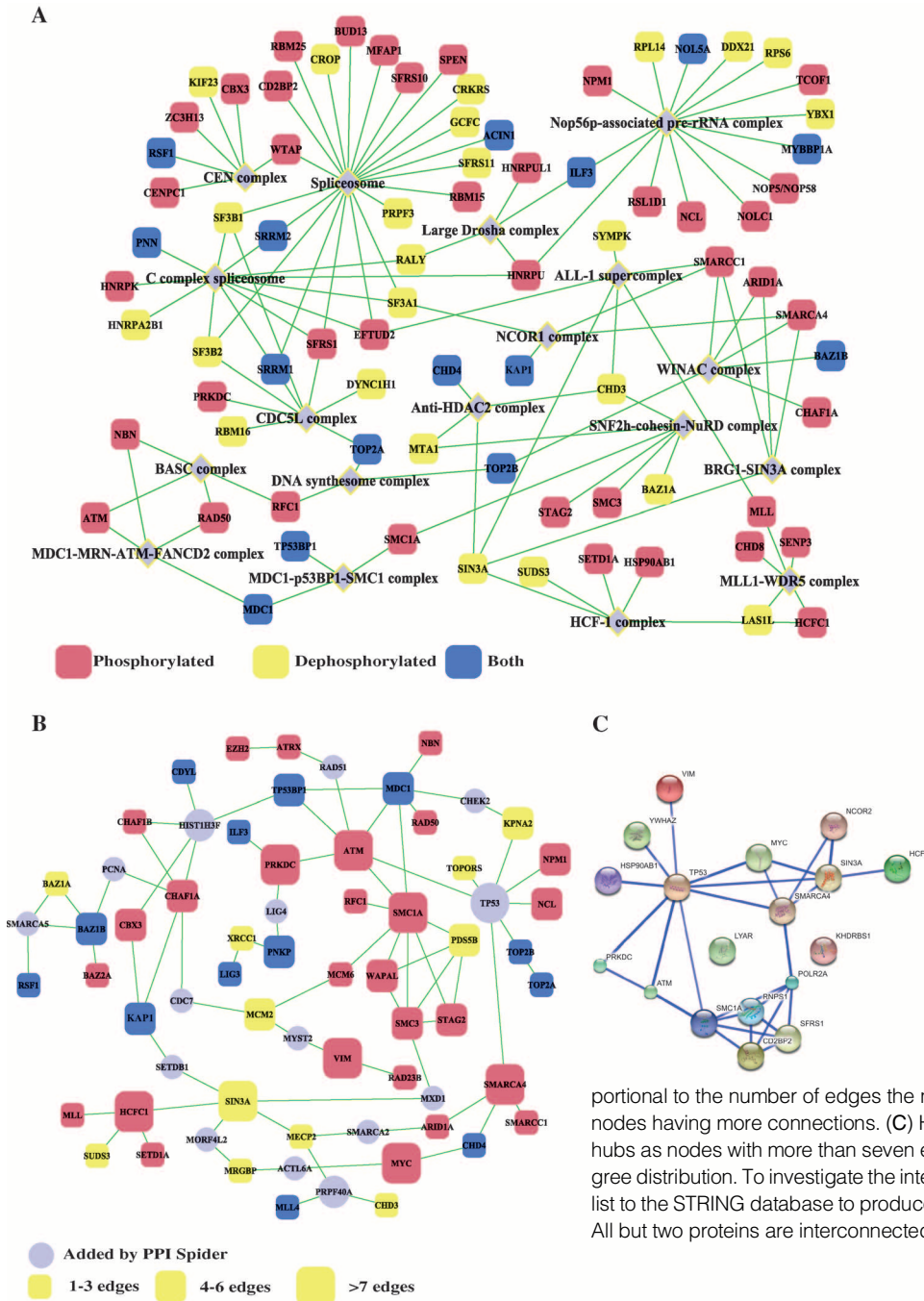


Fig. 3. Network analysis of the DSB-responsive phosphoproteome by molecular complexes and functional modules. **(A)** Selected complexes from the CORUM analysis. CORUM, a resource of manually annotated mammalian protein complexes, was used to identify complexes potentially involved in the DDR. Complexes selected contained at least two proteins from our lists. An expanded view of the network is shown in fig. S4. ALL-1 supercomplex, anti-HDAC2 complex, BRG1-SIN3A complex, MLL1-WDR5 complex, HCF-1 complex, NCOR1 complex, WINAC complex, and SNF2h-cohesin-NuRD complex are chromatin-modifying complexes involved, among other cellular processes, in transcriptional regulation; CEN complex, centromere chromatin complex, CDC5L complex, C complex spliceosome, and spliceosome are complexes involved in RNA splicing; BASC (BRCA1-associated genome surveillance complex), which may serve as a sensor for DNA damage, MDC1-MRN-ATM-FANCD2 complex, and MDC1-p53BP1-SMC1 complex are involved in DNA damage sensing and repair; DNA synthesome complex is involved in DNA synthesis and replication; large Drosha complex is involved in microRNA processing; and Nop56p-associated pre-ribosomal RNA complex is involved in ribosome biogenesis. **(B)** Functional module representing DNA Repair and Chromosome Organization identified by PPI Spider. The 245 proteins identified in this study were connected into a network containing 386 nodes (fig. S5). Functional modules in this network were sought by matching proteins in the network to specific biological processes using the GO tool BiNGO. The size of a node is proportional to the number of edges the node has in the full network (fig. S5), with larger nodes having more connections. **(C)** Hub nodes in the DDR PPI network. We defined hubs as nodes with more than seven edges, which represented the top 5% of the degree distribution. To investigate the interactions between these hubs, we submitted the list to the STRING database to produce the “core” network downloaded from STRING. All but two proteins are interconnected. Color and node size are arbitrary.

activate, directly or indirectly, certain phosphatases that are subsequently unaffected by ATM switch off. Searching for enriched kinase predictions, we found that the ATM-regulated and ATM-dependent phosphorylation and dephosphorylation events were enriched for similar kinase predictions (table S12). For example, like ATM-dependent phosphorylations, the ATM-regulated ones were enriched for predicted targets of PIKK (ATM, DNA-PK, and ATR) and for targets of NIK, CK2, and GRK2. Among the ATM-regulated dephosphorylation events, predicted targets of KIS, CDC2, and FRAP were enriched. Thus, the use of the ATMi in two different scenarios allowed us to identify fractions of the phosphorylation response to DNA damage that require ATM activity at various times in relation to damage induction. The analysis indicated that sustained ATM activity is required to maintain phosphorylation of some of its targets during the DDR and that ATM ac-

tivity may stimulate phosphatase activity early in the DDR, which may contribute to the requirement for sustained ATM activity.

Identification of a previously unknown damage-induced regulatory phosphorylation site on ATM

We carried out an in-depth analysis of one of the ATM-dependent phosphorylation sites that occurred on Ser²⁹⁹⁶ of ATM (fig. S7A), because DNA damage induces various posttranslational modifications of ATM that likely regulate its activity (28, 32, 72). We generated a phosphorylation-specific antibody against pSer²⁹⁹⁶ (fig. S7B) and monitored phosphorylation of this site under different conditions. The phosphorylation of Ser²⁹⁹⁶ was ATM-dependent and DNA-PK-independent (Fig. 5A and fig. S7C). The phosphorylation of Ser²⁹⁹⁶ exhibited a time course (Fig. 5B) different from that of the autophosphorylation of ATM on Ser¹⁹⁸¹ (28).

We established fibroblast cell lines that lacked endogenous ATM and stably expressed ectopic ATM (73) in wild-type and mutant (S2996A) versions; the mutant protein was nonphosphorylatable on Ser²⁹⁹⁶ (fig. S8A). Clonogenic survival assays indicated that cells expressing ATM-S2996A were more sensitive to NCS cytotoxicity than were cells expressing the wild-type protein (Fig. 5C). However, the S2996A substitution did not affect the efficiency of several ATM-mediated phosphorylations in response to DNA-damaging chemicals, including ATM's autophosphorylation on Ser¹⁹⁸¹ (fig. S8B). This suggests that ATM's activation and activity after damage induction was not impaired by ablating the Ser²⁹⁹⁶ phosphorylation site. We examined the recruitment of ATM to DSB sites and its retention there (74, 75) by fluorescence recovery after photobleaching analysis of yellow fluorescent protein (YFP)-tagged wild-type and mutant (S2996A) ATM after the induction of localized DNA damage (75). We found that the mutant had impaired retention at the damaged sites relative to wild-type ATM (Fig. 5D); the S2996A mutant behaved similarly to ATM with a mutation in the autophosphorylation site Ser¹⁹⁸¹ (75). This indicates that ATM's retention at damaged sites is affected jointly by at least two phosphorylation events.

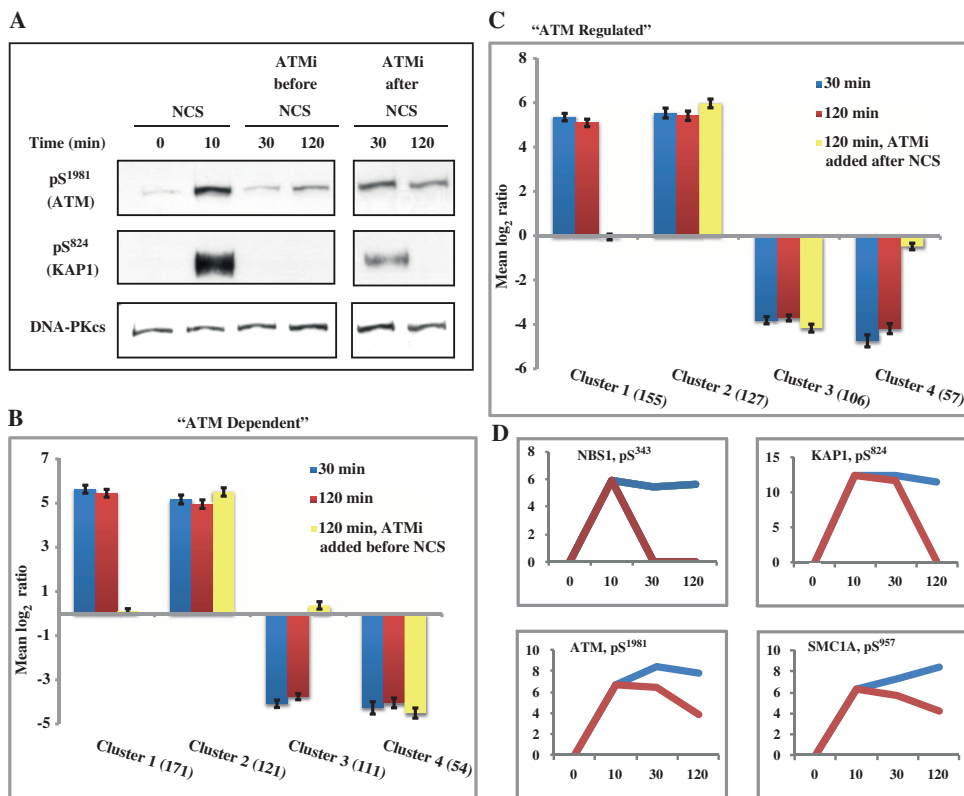


Fig. 4. Effect of the ATM inhibitor KU55933 (ATMi) on ATM-dependent phosphorylations. **(A)** Western blotting analysis showing autophosphorylation of ATM on Ser¹⁹⁸¹ and the ATM-dependent phosphorylation of the protein KAP1. ATMi was added either before NCS treatment or 15 min after NCS administration. DNA-PK served as the loading control. Blot shown is representative of the two experiments. **(B)** CLICK analysis showing the effect of adding ATMi before NCS treatment reveals DDR-induced phosphorylation changes that depend on ATM. Clusters are presented as bars representing the mean log₂ ratio ± SEM. In parentheses is the number of phosphorylation sites in each cluster. 30 min and 120 min represent samples collected at these times after NCS administration; 120 min ATMi added before NCS represents samples collected 120 min after NCS administration that had been exposed to ATMi 30 min before NCS. **(C)** CLICK analysis showing the effect of adding ATMi 15 min after the addition of NCS reveals DDR-induced phosphorylation changes that are regulated by ATM. Clusters are presented as in **(B)**. **(D)** Sustained activity of ATM is required to maintain specific ATM-dependent phosphorylations over time on Ser¹⁹⁸¹ of ATM, Ser⁸²⁴ of KAP1, Ser⁹⁵⁷ of SMC1 (35), and Ser³⁴³ of NBS1 (33). Time points are presented on the x axis, and mean log₂ ratios of the site between NCS-treated and untreated samples are presented on the y axis. Blue indicates cells treated with NCS only. Red indicates cells treated with NCS, followed by ATMi 15 min later.

DISCUSSION

We explored the dynamics of the nuclear phosphoproteome in the face of radiomimetic DNA damage using unbiased isolation of phosphopeptides followed by quantitative label-free LC-MS. We used an ATM inhibitor to distinguish between ATM-dependent and -independent components of these dynamics and explored ATM's role in maintaining the phosphorylation events over time. A complex response involving both

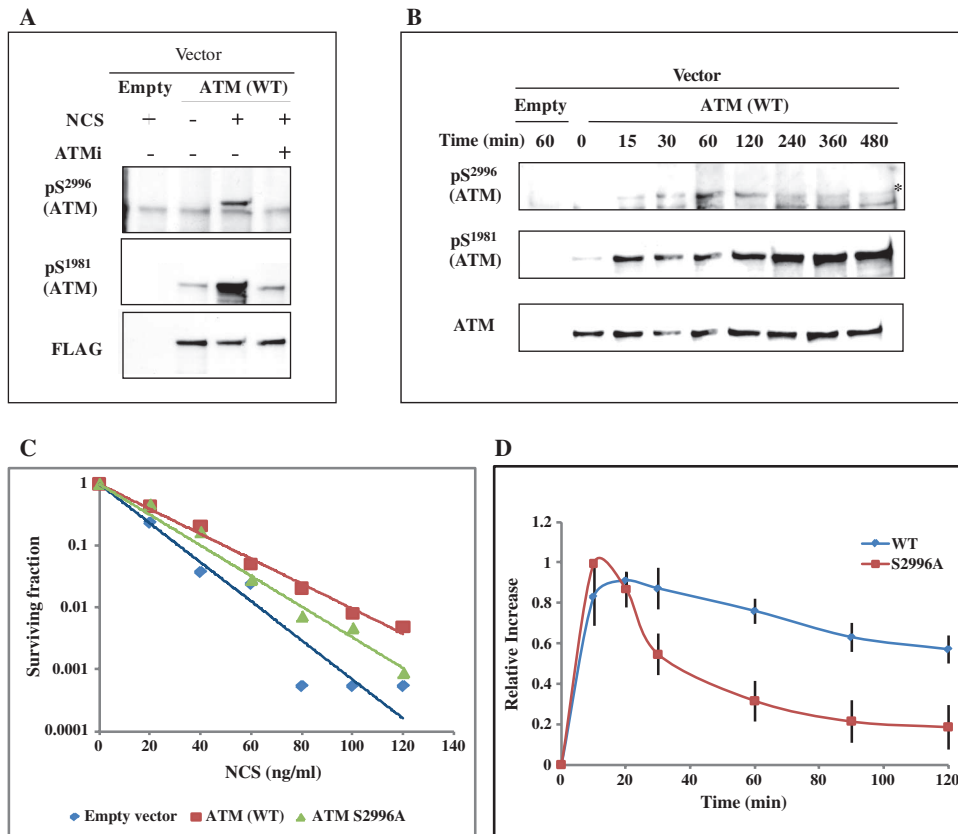


Fig. 5. Functional analysis of a damage-induced phosphorylation on Ser²⁹⁹⁶ of ATM. **(A)** ATM dependence of Ser²⁹⁹⁶ phosphorylation. Fibroblasts derived from an A-T patient, which are devoid of endogenous ATM, were transfected with empty vector or vector stably expressing ectopic FLAG-tagged ATM and treated for 1 hour with NCS (200 ng/ml). Where indicated, ATMi was added 30 min before NCS treatment. ATM was immunoprecipitated from cellular extracts with beads coupled to antibodies that recognize FLAG. Western blotting analysis of the immunoprecipitates was performed with the indicated antibodies. Phosphorylated Ser²⁹⁹⁶ is the upper band in the pS²⁹⁹⁶ (ATM) blot; the lower band is a cross-reactive band because it is present also in the nontransfected cells. **(B)** Time course comparison of damage-induced phosphorylation of Ser²⁹⁹⁶ and Ser¹⁹⁸¹ on ATM. Cells expressing ectopic, FLAG-tagged ATM were treated with NCS (200 ng/ml) and harvested at the indicated time points. The asterisk indicates the pS²⁹⁹⁶ form of ATM. Blots in (A) and (B) are representative of two experiments. **(C)** Cellular sensitivity to radiomimetic treatment of A-T cells expressing ectopic wild-type or mutant (S2996A) ATM. The indicated cells were treated with various NCS doses and their clonogenic survival was measured. Data points represent the average of three replicates. This experiment is representative of three independent experiments. **(D)** ATM recruitment at sites of laser-induced DNA damage. AT5BIVA (AT5) cells expressing wild-type YFP-ATM (blue) or YFP-ATM/S2996A (red) were microirradiated, and time-lapse imaging was used to collect the kinetic data. Each data point is the average of 10 independent measurements and a representative of two experiments.

increased and decreased phosphorylation was identified. In some cases, alterations in the amounts of phosphopeptides might reflect changes in protein amounts or subcellular localization. However, we attribute most of the damage-induced alterations that we detected to kinase-mediated phosphorylation events and phosphatase-mediated dephosphorylation events, because (i) we observed rapid kinetics for most of the phosphorylation events, which is typical for DSB-induced phosphorylations; (ii) data from previous studies found little overlap between proteome and phosphoproteome alterations (25, 76); and (iii) our results validated data obtained in previous phosphoproteomic screens (77–81).

The phosphorylation and dephosphorylation events that we recorded involved many interconnected proteins and protein complexes, attesting to a vigorous and comprehensive cellular response to DNA damage. Although the importance of protein phosphorylation in the DDR is well established, phosphatases have only recently come into the spotlight. Our data suggest two potential effects of phosphatase involvement in the DDR. The first is timing of signaling events presumably driven by the protein dephosphorylation, and the second is the effect by which dephosphorylation counteracts specific phosphorylation events—possibly serving as shutoff signals.

Clustering analysis revealed the temporal aspects of the phosphorylation and dephosphorylation response and grouped together events with similar temporal patterns. When combined with data obtained from experiments in the presence of an ATM inhibitor, this analysis provided an assessment of the degree of ATM dependence of the cellular protein phosphorylation response to radiomimetic damage. Although ATM is a major regulator of this response, the substantial fraction of ATM-independent events that we identified suggests that the DDR involves many kinases and supports the concept that, although ATM-mediated signaling is linked to a specific DNA lesion, DSBs, only a fraction of DSB repair is ATM-dependent (82). The substantial fraction of ATM-independent signaling in response to NCS-induced damage (expected to include a higher proportion of DSBs relative to damage caused by ionizing radiation) may reflect not only cellular responses to other types of DNA lesions induced by NCS, but may also reflect the DSB-mediated induction of ATM-independent stress responses.

The exploration of the DNA damage-induced dynamics of the nuclear phosphoproteome was not biased toward ATM and ATR substrates and, therefore, provides a broad perspective of the signaling dynamics elicited by such damage. The relatively

small proportion of phosphorylation events that occurred on the SQ/TQ motifs—the canonical targets of the PIKK family members—attests to the extended scope of the damage-induced phosphorylation landscape uncovered in this study. Although overlapping, but different, subsets of the phosphoproteome are identified following various enrichment methods (19), we do not expect the enrichment method that we used to be biased against pSQ- or pTQ-containing peptides. Seventy-five percent of the ATM-dependent increased phosphorylation events were not located in SQ/TQ motifs, indicating that many damage-responsive phosphorylation events are likely mediated by protein kinases that are ATM targets, directly

or indirectly. A well-documented example is the kinase CHK2 (83); other candidates that emerged from this study are CK2 and NIK (table S12). ATM presumably fine-tunes downstream processes by phosphorylating several proteins in each process, with additional ATM-dependent phosphorylation events on the same or other proteins carried out by protein kinases activated by ATM (3, 6).

We searched the target motifs of the DSB-responsive phosphorylation sites for known kinases in a statistically rigorous analysis. Some of the protein kinases highlighted by this analysis have been previously implicated in the DDR. CK2 is involved in the phosphorylation of several DDR proteins (84), is implicated in an early damage response (the phosphorylation and eviction of heterochromatin protein 1 β from chromatin) (85), and plays a role in the dynamic interaction of two DSB sensors, NBS1 and MDC1 (86, 87). The statistically significant enrichment for predicted CK2 kinase targets among ATM-dependent phosphorylation sites, as well as in Chromosome Organization proteins and Adenyl Ribonucleotide Binding proteins, suggests that CK2 may be a critical protein kinase in the DDR.

Phosphatases previously implicated in the DDR usually counteract specific phosphorylation events. Among them are PP5 (protein phosphatase 5) (88, 89), PP2A (90–92), WIP1 (wild-type p53-induced phosphatase 1) (93–95), and PP1 (96–98). Although prediction of phosphatase target sites is currently not possible, we attempted to identify the protein kinases whose action is counteracted by dephosphorylation after DNA damage. This analysis pointed to several kinases, including FRAP, CDKs, and MAPKs, which are involved in regulation of the cell cycle and other aspects of cellular proliferation. Note that the melanoma G361 cells that we used harbor a somatic mutation in the gene encoding the B-RAF protein, leading to a V600E substitution (99), which results in constitutive signaling by the MAPKs of the extracellular signal-regulated kinase (ERK) family (100) and makes the damage-induced abolishment of ERK-mediated phosphorylation particularly visible. Our analysis did point to CK2 targets in the sites that were dephosphorylated during the DDR. The enrichment of CK2 targets among dephosphorylated proteins is plausible, because CK2 is a constitutively active kinase (101, 102). Conceivably, CK2 may not be activated upon DNA damage but modulated to act on a certain set of targets, whereas some of its constitutive targets become dephosphorylated.

We integrated the proteins with altered phosphorylation status in response to DNA damage into several interconnected networks, which revealed cross talk among the different DDR branches. Although the intimate relationships between DNA repair and chromosome organization are self-explanatory, the integration of RNA-processing machineries into the DDR (Fig. 3 and figs. S4 and S6) is less so. However, the involvement of RNA-processing proteins in the DDR was demonstrated in a study that identified proteins involved in DDR in a genome-wide small interfering RNA screen (103). RNA binding and RNA-processing proteins were also identified in a proteomic screen for ATM or ATR substrates (13), and studies support a role for some of these proteins in the DDR (104, 105). These proteins may play a role in the DDR in their known capacity in RNA processing or may acquire a different function after their DNA damage-induced phosphorylation (29) (104). Our data indicate that in response to DNA damage, RNA-processing proteins are regulated by both phosphorylation and dephosphorylation events and that the corresponding sites are enriched for ATR and CK2a signatures, respectively. A relevant example is the CDC5L complex, represented in our study by several of its members. The CDC5L complex interacts with ATR, is involved in mRNA splicing, and is implicated in the processing of DNA interstrand cross-links *in vitro* (106, 107).

The efficiency of the ATM inhibitor in switching off ATM's activity (71) allowed us to identify the requirement of sustained ATM activity for the maintenance of many ATM-dependent phosphorylation events. Evi-

dence for the requirement of ongoing ATM activity after irradiation for preventing accumulation of chromosomal damage has been reported (71). Our data show at the systems level that ATM's control of many DDR processes is based on its sustained activity over an extended period after damage induction. This observation suggests that ATM's duty is not just to “touch (the substrate) and go,” but to stay and maintain the phosphorylation of its targets, probably in the face of opposing dephosphorylating activities. Such an antagonistic circuit regulates the protein kinase Chk1 by ATR and the phosphatase PP2A (108). However, phosphatases may not always terminate signaling, because inhibition of PP2A led to ATM autophosphorylation on Ser¹⁹⁸¹, a marker of ATM activation (28, 92). Perhaps the best-documented phosphatase that counteracts DNA damage-induced phosphorylations is WIP1 (also known as PPM1D), which dephosphorylates phosphorylation sites on key proteins in the DDR, including those of p53, MDM2, MDMx, CHK1, ATM itself, γ H2AX, and probably additional sites containing the SQ/TQ motifs (93, 94, 109–115). WIP1 is also involved in the negative feedback of the dynamic regulation of p53 by ATM (116). The interplay between phosphorylation and dephosphorylation is a central mechanism in the fine-tuning of many signaling networks (117, 118) and may be part of the mechanism by which the DDR decays in a timely manner after damage repair, allowing the cellular life cycle to resume. Some of the responsible phosphatases may be activated by ATM itself in a negative feedback mechanism. ATM activates at least one phosphatase, PP1, by phosphorylating and thereby inactivating an inhibitory subunit of this enzyme (97).

Finally, we validated and examined the function of a previously unknown DNA damage-induced, ATM-dependent phosphorylation on ATM itself at Ser²⁹⁹⁶. There are previously documented autophosphorylation sites, a CDK5-mediated phosphorylation site, and a Tip60-mediated acetylation event on activated ATM (28, 32, 119, 120). In the ATM amino acid sequence, Ser²⁹⁹⁶ is followed by an aspartic acid residue; hence, it is not a typical ATM target. However, the Ser¹⁸⁹³ autophosphorylation site on ATM is followed by an acidic residue, glutamic acid (32); thus, it is possible that Ser²⁹⁹⁶ phosphorylation is carried out by ATM itself. The role of autophosphorylation in ATM activation has been debated (28, 32, 121, 122), and at least the autophosphorylation on Ser¹⁹⁸¹ is required for ATM retention on chromatin (75) at DSB sites (74). The phosphorylation event that we identified on Ser²⁹⁹⁶ appears to play a role in the same process (Fig. 5D), suggesting that ATM retention is modulated by several phosphorylation events. ATM's retention at site of DNA damage is presumably important for sustained phosphorylation of substrates recruited to those sites (4, 5). In view of our finding that sustained ATM activity is required for maintaining certain phosphorylation events, it is conceivable that ATM's retention at damaged sites is important for maintaining specific phosphorylation events at those sites.

Bennetzen *et al.* (123) published data from a similar experimental setup in which they too observed the complexity of the DNA damage-induced phosphoproteome dynamics without addressing its ATM dependence. Our study expands the DDR landscape and identifies previously unknown ATM-dependent and -independent branches and reveals a complex cellular response to stimuli. This complexity and the involvement of the DDR in numerous aspects of cellular survival are in line with the critical importance of genomic stability in maintenance of cellular homeostasis.

MATERIALS AND METHODS

Reagents

Chemicals of the highest available purity were purchased from Sigma-Aldrich unless otherwise stated. The ATM inhibitor KU55933 (70) and

the DNA-PK inhibitor NU-7441 (*I24*) were obtained from Tocris. The radiomimetic chemical NCS, camptothecin, and hydroxyurea were obtained from Sigma-Aldrich.

Cell culture

G361 human melanoma cells (American Type Culture Collection, CRL-1424) were grown in McCoy's 5A Modified Medium (Invitrogen) supplemented with 10% fetal calf serum (FCS) and antibiotics. AT221JE-T, an SV40 (simian virus 40)-immortalized fibroblast cell line derived from an A-T patient (*73*), was grown in Dulbecco's modified Eagle's medium (DMEM) (Invitrogen) supplemented with 15% FCS and antibiotics. The ATM-deficient AT5BIVA cell line was grown in DMEM (Invitrogen) supplemented with 10% FCS and antibiotics.

Sample preparation for phosphoproteomics

For each condition, three 15-cm dishes of G361 cells were grown to ~90% confluence. Cells were treated with NCS at a final concentration of 200 ng/ml. The ATM inhibitor KU55933 (*70*) was added at a final concentration of 10 μ M. At various time points after NCS addition, the cultures were washed twice and the cells were scraped in ice-cold phosphate-buffered saline, spun down for 5 min at 300g, resuspended in hypotonic buffer [10 mM Hepes (pH 8.0), 10 mM KCl, 0.1 mM EDTA, and 0.1 mM EGTA] containing protease and phosphatase inhibitor cocktails (Sigma), and left on ice for 30 min. Cell membranes were disrupted by brief vortexing. Enriched nuclear fractions were collected by centrifugation for 10 min at 10,000g. Nuclear pellets were washed once in hypotonic buffer and resuspended in 8 M urea solution containing 0.1 M ammonium bicarbonate, and the resulting extracts were spun for 10 min at 37°C and 1400 rpm in a Thermomixer (Eppendorf). The BCA (bicinchoninic acid) Protein Assay (Pierce) was used to measure protein concentration.

Phosphopeptide enrichment

Disulfide bonds were reduced with tris(2-carboxyethyl)phosphine at a final concentration of 10 mM at 37°C for 1 hour. Free thiols were alkylated with 20 mM iodoacetamide at room temperature for 30 min in the dark. The excess of iodoacetamide was quenched with *N*-acetyl cysteine at a final concentration of 25 mM for 15 min at room temperature. The solution was subsequently diluted with 20 mM tris-HCl (pH 8.3) to a final concentration of 1.0 M urea and digested overnight at 37°C with sequencing-grade modified trypsin (Promega) at a protein-to-enzyme ratio of 50:1. Peptides were desalted on a C18 Sep-Pak cartridge (Waters) and dried under vacuum. Before the experiments, we evaluated two resins for selective phosphopeptide enrichment and found that titanium dioxide (TiO₂) best suited our purpose. Phosphopeptides were isolated from 2 mg of total peptide mass with TiO₂ as described previously (*19*, *125*). Briefly, the dried peptides were dissolved in an 80% acetonitrile (ACN)–2.5% trifluoroacetic acid (TFA) solution saturated with phthalic acid. Peptides were added to the same amount of equilibrated TiO₂ (5- μ m bead size, GL Science) in a blocked Mobicol spin column (MoBiTec) that was incubated for 30 min with end-over-end rotation. The column was washed twice with the saturated phthalic acid solution, twice with 80% ACN and 0.1% TFA, and finally twice with 0.1% TFA. The peptides were eluted with a 0.3 M NH₄OH solution. The pH of the eluates was adjusted to 2.7 with 10% TFA solution, and phosphopeptides were again desalted with microspin C18 cartridges (Harvard Apparatus).

LC-MS/MS analysis

Chromatographic separation of peptides was carried out with an Eksigent NanoLC system (Eksigent Technologies) connected to a 15-cm fused-silica emitter with 75- μ m inner diameter (BGB Analytik) packed in-house with

a Magic C18 AQ 3- μ m resin (Michrom BioResources). Aliquots (1 μ g) of total phosphopeptide sample were analyzed by LC–tandem MS (LC-MS/MS) run with a linear gradient ranging from 98% solvent A (0.15% formic acid) and 2% solvent B (98% ACN, 2% water, and 0.15% formic acid) to 30% solvent B over 90 min at a flow rate of 300 nL/min. Mass spectrometric analysis was performed with a 7 T Finnigan LTQ FT-ICR (Fourier transform ion cyclotron resonance) instrument (Thermo Electron) equipped with a nanoelectrospray ion source (Thermo Electron). Each MS1 scan (acquired in the ICR cell) was followed by collision-activated dissociation (CAD, acquired in the LTQ part) of the three most abundant precursor ions with dynamic exclusion for 20 s. Total cycle time was ~1 s. For MS1, 10⁶ ions were accumulated in the ICR cell over a maximum time of 300 ms and scanned at a resolution of 100,000 full width at half maximum [at 400 mass/charge ratio (*m/z*)]. MS2 scans were acquired with the normal scan mode, a target setting of 10⁴ ions, and an accumulation time of 250 ms. Singly charged ions and ions with unassigned charge states were excluded from triggering MS2 events. The normalized collision energy was set to 32%, and one microscan was acquired for each spectrum.

Database searching

The fragment ion spectra were queried against the International Protein Index (IPI) human database (release 3.26 containing 66,524 entries) using the SORCERER-SEQUENT (v. 3.0.3) (*126*), which was run in the SageN Sorcerer2 (Thermo Electron). For in silico digestion, trypsin was used as the protease and was assumed to cleave after lysine (K) and arginine (R) unless followed by proline (P). Two missed cleavage sites and one non-tryptic terminus were allowed per peptide, and the maximal peptide mass was limited to 4500 daltons. The precursor ion tolerance was set to 15 parts per million (ppm), and fragment ion tolerance was set to 0.5 dalton. The data were searched allowing phosphorylation (+79.9663 daltons) of serine, threonine, and tyrosine as a variable modification and carboxyamidomethylation of cysteine (+57.0214 daltons) residues as a fixed modification. Finally, the database search results obtained by SEQUEST were subjected to statistical analysis with the PeptideProphet algorithm (v. 3.0) (*127*). The X correlation score (Xcorr) of the first and the second ranked hits for a tandem mass spectrum as determined by SEQUEST were used to compute the dCn (delta correlation score), enabling estimation of the accuracy of phosphorylation site location (*128*). A phosphopeptide with a dCn >0.125 was considered to have a correctly located phosphorylation site. The false-positive rate (FPR) for phosphopeptide assignments was kept below 2%.

Label-free quantification

For the detection of the peptide features that differed in abundance between samples, the in-house developed software system SuperHirn (*129*) was used for extraction, de-isotoping, peak integration, and alignment of detected features over multiple LC-MS runs. Finally, each feature was matched with the best peptide assignment obtained after database searching. The generated intensity map containing all aligned features, together with the corresponding peptide sequences (called “MasterMap”), was further filtered and processed with the Spotfire Decision Site program (TIBCO). Only phosphopeptides having a PeptideProphet score of more than 0.9, corresponding to an FDR of less than 1%, were selected. Two MasterMaps were generated for these experiments (full list of samples is in table S1).

Data processing and peptide filtering

Each MasterMap was processed to generate final fold-change ratios in peptide amounts between treated and untreated samples for each time point. Feature intensity values that were missing in the data matrix were addressed according to (*130*). Briefly, we set a nominal lower bound value

as the minimum measured intensity and replaced with it missing values and values below it. We then calculated fold-change ratios between treated and untreated samples. Because replicates were collected on different days, we calculated the fold-change ratio for each treated sample relative to an average value of the untreated samples from the same day, and then averaged these ratios. The final data matrix included a single \log_2 fold-change ratio for each time point.

Next, we identified phosphopeptides that changed in abundance in response to DSB induction. For this purpose, and to assess the amount of noise in our data set, we created a “mock data set” by calculating fold-change ratios between untreated samples recorded on the same day. We then applied a filtering criterion to the data sets (real and mock) composed of a fold-change threshold and a cutoff for the number of samples in which the peptide’s ratio was above that threshold. The two data sets were filtered by several criteria to assess the signal-to-noise ratios of each criterion. Ratios between the number of peptides passing different criteria settings in the real and mock data sets were calculated. We further refined our filtering scheme by taking advantage of the fact that time course experiments provide an ordering of the samples. Thus, to incorporate the aspect of time and reduce the amount of noise, we further filtered the data set for features regulated in consecutive samples (fig. S1B). This improved the signal-to-noise ratio more than increasing the fold-change threshold. A good signal-to-noise estimate (14.6 for true/mock) was obtained for the criterion, which required a fourfold-change threshold (treated/untreated cells) in at least two consecutive time points. We saw no substantial improvement beyond this criterion in the signal-to-noise ratio, but only a reduction in the number of peptides passing the filter, when the fold-change threshold was increased. When a regulated phosphorylation site was found in several redundant phosphopeptides, we selected the peptide with fewer missing value entries.

Functional annotation

For functional annotation and GO enrichment analysis of protein sets, we used the annotation tools DAVID (30) and BiNGO (version 2.3) (59). The P value threshold was set at 0.01 after the FDR correction for multiple testing (Benjamini-Hochberg) for both tools. DAVID was the main tool for associating gene IDs to GO terms. BiNGO was used to analyze protein networks in Cytoscape (v. 2.6.2) (46).

Kinase-substrate relationship prediction

We compared the phosphorylation sites that we identified with known sites from the phospho.ELM (v. 8.2) (40) database and a phosphorylation data set from PhosphoSitePlus (<http://www.phosphosite.org>) (41). Kinase-substrate relationships were also downloaded from both databases. Mapping of known data to our data set was carried out in Spotfire (TIBCO). To predict protein kinases potentially involved in the DDR, including those responsible for phosphorylation sites that decreased in response to DNA damage, we used GPS (v. 2.1) (42). GPS uses well-established rules to classify protein kinases, uses a prediction that utilizes the kinase family hierarchy, and has a simple approach to estimate the theoretically maximal FPR. Downloaded GPS was used as a stand-alone program, and all predictions were made at high stringency. For serine-threonine kinases, the high threshold was established with an FPR of 2%. Enrichment tests used the hypergeometric distribution. As a background in these tests, we used large-scale prediction of all phosphorylation sites found in phospho.ELM (v. 8.2), complemented by the prediction of sites found in our data set and missing from the database. The P value cutoff for enrichment was set at 5×10^{-5} . Because GPS uses a prediction of protein kinases in hierarchy, we focused on the most detailed kinase or group. A complete list of enriched kinase predictions is available in the Supplementary Materials.

Motif analysis

To identify sequence motifs in our phosphorylation data set, we took the 15–amino acid sequence centered around the phosphorylation sites and, with the software tool Motif-X (31), extracted overrepresented patterns in a given sequence data set. The algorithm in this program uses an iterative strategy that builds successive motifs through comparison to a dynamic statistical background. The 15–amino acid sequences were loaded as pre-aligned text data, motifs were searched using standard parameters, and all motifs were identified with P values $<10^{-6}$ with the complete human IPI protein database as background. We searched for overrepresented motifs around serine and threonine residues. Because the kinase prediction analysis is based essentially on sequence motifs, we tested the relationship between overrepresented sequence motifs found by Motif-X and enriched kinase predictions found by our analysis. The test was performed by removing the phosphorylation sites with a certain sequence motif found by Motif-X from a list, retesting the list for enrichment, and comparing the enriched predicted kinases between the original and the subtracted lists. The removal of phosphorylation sites with a certain motif was expected to have the greatest effect on the kinase predictions to which this motif is linked. This analysis further refined the list of significantly enriched motifs found by Motif-X.

Cluster analysis

To cluster temporal or regulatory patterns of phosphorylation sites, we used the clustering algorithm CLICK implemented in the microarray analysis suite EXPANDER (44). CLICK uses graph-theoretic and statistical techniques to identify tight groups of similar elements that are likely to belong to the same cluster. Before clustering, rows (\log_2 ratios for each phosphorylation site) were standardized to mean 0 and SD 1, because, in our analysis, elements were considered similar if they shared response patterns even if they differed in the magnitude of response. For the analysis of kinetics, we included only the clusters of phosphorylation sites with smooth trend lines of the average. That is, we excluded patterns in which at one of the time points (30 or 120 min), the average was substantially different from that at the other time points.

CORUM analysis

CORUM (47) (September 2009 release), a resource of manually annotated mammalian protein complexes, was used to identify complexes potentially involved in the DDR. CORUM’s core data set was converted to a binary format (complex-protein) and uploaded to Cytoscape. The complex-protein interaction map provided a simplified view of the PPI map and allowed us to highlight key players and complexes for which the phosphorylation status was regulated by DNA damage. We chose complexes that were implicated by at least two subunits from our list. Only proteins identified from our list are presented in the final figures.

Network analysis

For a preliminary view of interconnected proteins within our list, we submitted it to the STRING (v. 8.3) database (45) and filtered for interactions of high confidence (score >0.7). Interaction data were downloaded and processed with Cytoscape. To connect more proteins and to assign statistical significance to this analysis, we submitted our protein list to PPI Spider (48). PPI Spider implements a robust statistical framework for the interpretation of protein lists in the context of a global PPI network. The input list is translated into a network model according to the topology of the PPI network. PPI Spider’s output is a model of protein interactions that represents the statistically most probable connections among proteins in the list. One thousand random networks were used as background. Model D2, which allows one unknown intermediate protein

between every two proteins from our list, was used, and the *P* value for the model was <0.001. The model was downloaded as a text file, subsequently uploaded onto Cytoscape, and queried for significant biological processes with BiNGO 2.3 and DAVID. To construct a functional module, we identified all proteins annotated to a certain biological process with BiNGO. The shortest path connecting these proteins was chosen in any given network. Only the minimal set of nodes and edges required to connect these annotated proteins was selected for the description of a functional module. Topological parameters of the network were calculated with the Cytoscape plug-in CentiScaPe (49).

Protein analysis

For Western blotting, cells were lysed for 30 min at 4°C in 50 mM tris-HCl (pH 7.5), 150 mM NaCl, 1% (v/v) Igepal (NP-40 analog), and 1 mM EDTA supplemented with a protease and phosphatase inhibitor mixture. Supernatants were collected after centrifugation at 21,000g for 20 min, and protein concentration was determined with the Bradford method (Bio-Rad). Cellular extracts (80 to 150 µg) were separated on SDS–polyacrylamide gel electrophoresis and transferred overnight at 4°C onto a polyvinylidene difluoride membrane (Amersham Pharmacia Biotech). Membranes were blocked for 40 min in 5% dry milk in Tween–tris-buffered saline (TTBS) and incubated overnight at 4°C with a primary antibody diluted in TTBS containing 1% bovine serum albumin.

For ATM immunoprecipitation, cells were lysed for 30 min at 4°C in 50 mM tris-HCl (pH 7.5), 150 mM NaCl, 1% (v/v) Igepal, 0.5% (v/v) DOC (deoxycholate), 0.1% (v/v) SDS, 1 mM dithiothreitol, and 1 mM EDTA supplemented with a protease inhibitor mixture (Roche) and a phosphatase inhibitor mixture (Sigma). Supernatants were collected after centrifugation at 21,000g for 10 min and incubated for 3 hours with pre-washed anti-FLAG M2 beads (Sigma). Beads were then washed three times with lysis buffer and boiled in sample buffer.

The following primary antibodies were used: antibodies against pS¹⁹⁸¹/ATM, NBS1 (Epitomics), ATM (MAT3, Sigma), FLAG (Sigma), HSC70, glyceraldehyde-3-phosphate dehydrogenase (GAPDH), LAMB1 (Santa Cruz Biotechnology), pSer²⁰⁵⁶/DNA-PKcs (Abcam), DNA-PKcs, pSer⁸²⁴/KAP1, pSer⁹⁶⁶/SMC1 (all from Bethyl Laboratories), and SMC1 (a gift from K. Yokomori). A phosphorylation-specific polyclonal antibody against pSer²⁹⁹⁶ of ATM was raised by Bethyl Laboratories.

Vectors and in vitro mutagenesis

The pEBS7 FLAG-ATM expression construct was previously described (73). pcDNA 3.1 FLAG-ATM was a gift from M. Kastan. pcDNA 3.1 YFP-FLAG-ATM was previously described (75). The mutation leading to the S2996A substitution in ATM was introduced into a construct containing an ATM fragment spanning the mutation site with the QuikChange Mutagenesis Kit (Stratagene). The mutated fragment subsequently replaced the corresponding wild-type fragment in the ATM expression vector, using flanking restriction sites of Bpu 1102I and Xho I.

Generation of cell lines stably expressing various versions of ATM

Transfection of the A-T cell line AT22IJE-T for the establishment of cell clones stably expressing various versions of ATM was carried out as previously described (73). Cells were added at 250,000 cells per well to a six-well plate and were transfected with 2 µg of DNA (empty pEBS7 vector or pEBS7 expressing wild-type or mutant S2996A ATM). Selection was carried out with hygromycin B (100 µg/ml) in F10 medium containing 20% FCS for 2 weeks, and the cultures were subsequently grown in DMEM with 15% FCS.

Cellular sensitivity to radiomimetic treatment

For clonogenic survival assays, fibroblasts at the logarithmic phase were replated at densities of 200 to 20,000 cells per 6-cm dish. The next day, cells were treated with varying doses of NCS and incubated for 12 to 14 days in Ham's F-10 medium supplemented with 20% FCS. Cell colonies were fixed and stained with 2% (w/v) crystal violet in 50% ethanol. Colonies of at least 50 cells were scored. The surviving fraction for each NCS dose was calculated and survival curves were constructed.

Live-cell imaging and laser micro-irradiation

Live cell imaging combined with laser micro-irradiation were performed as described previously (75, 131). Briefly, YFP-ATM was expressed by transfection of AT5BIVA cells with Amara (Lonza). Laser micro-irradiation and imaging were performed at 48 hours after transfection. DSBs were introduced in the nuclei of cultured cells by micro-irradiation with a pulsed nitrogen laser (Spectra-Physics; 365 nm, 30-Hz pulse), as previously described (131). The laser system (Micropoint Ablation Laser System; Photonic Instruments Inc.) was coupled directly to the epifluorescence path of the microscope (Axiovert 200M, Carl Zeiss Microimaging Inc.) for time-lapse imaging. During micro-irradiation, imaging, or analysis, the cells were maintained at 37°C in 35-mm glass-bottom culture dishes (MatTek Cultureware). The growth medium was replaced by CO₂-independent medium (Invitrogen) with 10% serum before analysis. Images were made with an Axiovert 200 M microscope, equipped with an AxioCam HRm, with a Plan-Apochromat 63× 1.4 numerical aperture (NA) oil immersion objective. Time-lapse image acquisition was started before laser micro-irradiation to obtain an image of the unirradiated cell. DSBs were introduced in cell nuclei by micro-irradiation with the pulsed nitrogen laser at the time of the second image. Exposure time was set at 40 ms, allowing five laser pulses to hit a defined region in a single nucleus. To compensate for nonspecific photobleaching, we subtracted the background fluorescence from the accumulation spot. Relative fluorescence (RF) intensity was calculated by the following formula: $RF(t) = (I_t - I_{preIR}) / (I_{max} - I_{preIR})$, where I_{preIR} represents the fluorescence intensity of micro-irradiated area before irradiation, and I_{max} represents the maximum fluorescence signal in the micro-irradiated area. Fold increase (FI) was calculated by the following formula: $FI(t) = I_t / I_{preIR}$. Each data point was the average of 10 independent measurements.

SUPPLEMENTARY MATERIALS

www.sciencesignaling.org/cgi/content/full/3/151/rs3/DC1

Fig. S1. Schematic workflow and estimation of signal-to-noise criteria for fold-change filtering.

Fig. S2. Time course data set analyzed for overrepresented sequence motifs, as well as known kinase-substrate relationships.

Fig. S3. PPI network of the DDR phosphoproteome obtained with STRING.

Fig. S4. Full network view of the protein complexes associated with DDR phosphoproteome identified by CORUM analysis.

Fig. S5. Full network view of the PPI network of the DDR phosphoproteome identified by PPI Spider analysis.

Fig. S6. Properties of the PPI Spider protein-protein interaction network of the DDR phosphoproteome.

Fig. S7. pSer²⁹⁹⁶ on ATM, identified by MS/MS and a phosphorylation-specific antibody, is DNA-PK-independent.

Fig. S8. The S2996A mutation in ATM does not affect ATM-dependent phosphorylations after DNA damage induction.

Table S1. List of samples (biological replicates) used for the two MasterMaps.

Table S2. DNA damage-responsive phosphorylation events in the time course data set.

Table S3. Significant GO terms extracted from DAVID.

Table S4. DNA damage-responsive phosphorylation sites with a known kinase identified in databases.

Table S5. Kinase prediction enrichment analysis of phosphorylation sites and the association with Motif-X motifs.

Table S6. Kinase prediction enrichment analysis coupled to DAVID GO analysis.

Table S7. Kinase prediction enrichment analysis coupled to CLICK clustering analysis.
 Table S8. DAVID GO analysis of CLICK clusters.
 Table S9. Protein complexes depicted by CORUM in the protein lists obtained in this study.
 Table S10. Effect of the PPI Spider network generation procedure on the analysis of GO term enrichment.
 Table S11. DNA damage-responsive phosphorylation events in the ATM dependence data set.
 Table S12. Kinase prediction enrichment analysis of the ATM dependence data set.
 Table S13. Complete list of phosphorylation sites identified in this study.
 Table S14. Complete list of phosphopeptides identified in this study.

REFERENCES AND NOTES

1. T. T. Su, Cellular responses to DNA damage: One signal, multiple choices. *Annu. Rev. Genet.* **40**, 187–208 (2006).
2. C. H. Bassing, F. W. Alt, The cellular response to general and programmed DNA double strand breaks. *DNA Repair* **3**, 781–796 (2004).
3. M. F. Lavin, S. Kozlov, ATM activation and DNA damage response. *Cell Cycle* **6**, 931–942 (2007).
4. S. Bekker-Jensen, C. Lukas, R. Kitagawa, F. Melander, M. B. Kastan, J. Bartek, J. Lukas, Spatial organization of the mammalian genome surveillance machinery in response to DNA strand breaks. *J. Cell Biol.* **173**, 195–206 (2006).
5. J. W. Harper, S. J. Elledge, The DNA damage response: Ten years after. *Mol. Cell* **28**, 739–745 (2007).
6. Y. Shiloh, The ATM-mediated DNA-damage response: Taking shape. *Trends Biochem. Sci.* **31**, 402–410 (2006).
7. H. H. Chun, R. A. Gatti, Ataxia-telangiectasia, an evolving phenotype. *DNA Repair* **3**, 1187–1196 (2004).
8. M. F. Lavin, Ataxia-telangiectasia: From a rare disorder to a paradigm for cell signalling and cancer. *Nat. Rev. Mol. Cell Biol.* **9**, 759–769 (2008).
9. K. A. Cimprich, D. Cortez, ATR: An essential regulator of genome integrity. *Nat. Rev. Mol. Cell Biol.* **9**, 616–627 (2008).
10. C. A. Lovejoy, D. Cortez, Common mechanisms of PIKK regulation. *DNA Repair* **8**, 1004–1008 (2009).
11. A. Zajayeri, J. Falck, C. Lukas, J. Bartek, G. C. Smith, J. Lukas, S. P. Jackson, ATM- and cell cycle-dependent regulation of ATR in response to DNA double-strand breaks. *Nat. Cell Biol.* **8**, 37–45 (2006).
12. E. Callén, M. Jankovic, N. Wong, S. Zha, H. T. Chen, S. Difiillipantonio, M. Di Virgilio, G. Heidkamp, F. W. Alt, A. Nussenzweig, M. Nussenzweig, Essential role for DNA-PKcs in DNA double-strand break repair and apoptosis in ATM-deficient lymphocytes. *Mol. Cell* **34**, 285–297 (2009).
13. S. Matsuoaka, B. A. Ballif, A. Smogorzewska, E. R. McDonald III, K. E. Hurov, J. Luo, C. E. Bakalarski, Z. Zhao, N. Solimini, Y. Lerenthal, Y. Shiloh, S. P. Gygi, S. J. Elledge, ATM and ATR substrate analysis reveals extensive protein networks responsive to DNA damage. *Science* **316**, 1160–1166 (2007).
14. M. S. Huen, J. Chen, The DNA damage response pathways: At the crossroad of protein modifications. *Cell Res.* **18**, 8–16 (2008).
15. Y. Sun, X. Jiang, B. D. Price, Tip60: Connecting chromatin to DNA damage signaling. *Cell Cycle* **9**, 930–936 (2010).
16. J. R. Morris, SUMO in the mammalian response to DNA damage. *Biochem. Soc. Trans.* **38**, 92–97 (2010).
17. J. J. Mu, Y. Wang, H. Luo, M. Leng, J. Zhang, T. Yang, D. Besusso, S. Y. Jung, J. Qin, A proteomic analysis of ataxia telangiectasia-mutated (ATM)/ATM-Rad3-related (ATR) substrates identifies the ubiquitin-proteasome system as a regulator for DNA damage checkpoints. *J. Biol. Chem.* **282**, 17330–17334 (2007).
18. J. V. Olsen, B. Blagoev, F. Gnäd, B. Macek, C. Kumar, P. Mortensen, M. Mann, Global, in vivo, and site-specific phosphorylation dynamics in signaling networks. *Cell* **127**, 635–648 (2006).
19. B. Bodenmiller, L. N. Mueller, M. Mueller, B. Dorn, R. Aebersold, Reproducible isolation of distinct, overlapping segments of the phosphoproteome. *Nat. Methods* **4**, 231–237 (2007).
20. B. Bodenmiller, L. N. Mueller, P. G. Pedrioli, D. Pflieger, M. A. Junger, J. K. Eng, R. Aebersold, W. A. Tao, An integrated chemical, mass spectrometric and computational strategy for (quantitative) phosphoproteomics: Application to *Drosophila melanogaster* Kc167 cells. *Mol. Biosyst.* **3**, 275–286 (2007).
21. A. Gruhler, J. V. Olsen, S. Mohammed, P. Mortensen, N. J. Faergeman, M. Mann, O. N. Jensen, Quantitative phosphoproteomics applied to the yeast pheromone signaling pathway. *Mol. Cell. Proteomics* **4**, 310–327 (2005).
22. H. Daub, J. V. Olsen, M. Bairlein, F. Gnäd, F. S. Oppermann, R. Körner, Z. Greff, G. Kéri, O. Stemmann, M. Mann, Kinase-selective enrichment enables quantitative phosphoproteomics of the kinome across the cell cycle. *Mol. Cell* **31**, 438–448 (2008).
23. S. Morandell, T. Stasyk, S. Skvortsov, S. Ascher, L. A. Huber, Quantitative proteomics and phosphoproteomics reveal novel insights into complexity and dynamics of the EGFR signaling network. *Proteomics* **8**, 4383–4401 (2008).
24. M. W. Pinkse, S. Mohammed, J. W. Gouw, B. van Breukelen, H. R. Vos, A. J. Heck, Highly robust, automated, and sensitive online TiO₂-based phosphoproteomics applied to study endogenous phosphorylation in *Drosophila melanogaster*. *J. Proteome Res.* **7**, 687–697 (2008).
25. M. Hilger, T. Bonaldi, F. Gnäd, M. Mann, Systems-wide analysis of a phosphatase knock-down by quantitative proteomics and phosphoproteomics. *Mol. Cell. Proteomics* **8**, 1908–1920 (2009).
26. V. Nguyen, L. Cao, J. T. Lin, N. Hung, A. Ritz, K. Yu, R. Jianu, S. P. Ulin, B. J. Raphael, D. H. Laidlaw, L. Brossay, A. R. Salomon, A new approach for quantitative phosphoproteomic dissection of signaling pathways applied to T cell receptor activation. *Mol. Cell. Proteomics* **8**, 2418–2431 (2009).
27. K. Savitsky, A. Bar-Shira, S. Gilad, G. Rotman, Y. Ziv, L. Vanagaite, D. A. Tagle, S. Smith, T. Uziel, S. Sfez, M. Ashkenazi, I. Pecker, M. Frydman, R. Harnik, S. R. Patanjali, A. Simmons, G. A. Ciines, A. Sartieli, R. A. Gatti, L. Chessa, O. Sanal, M. F. Lavin, N. G. Jaspers, A. M. Taylor, C. F. Arlett, T. Miki, S. M. Weissman, M. Lovett, F. S. Collins, Y. Shiloh, A single ataxia telangiectasia gene with a product similar to PI-3 kinase. *Science* **268**, 1749–1753 (1995).
28. C. J. Bakkenist, M. B. Kastan, DNA damage activates ATM through intermolecular autophosphorylation and dimer dissociation. *Nature* **421**, 499–506 (2003).
29. Y. Ziv, D. Bielopolski, Y. Galanty, C. Lukas, Y. Taya, D. C. Schultz, J. Lukas, S. Bekker-Jensen, J. Bartek, Y. Shiloh, Chromatin relaxation in response to DNA double-strand breaks is modulated by a novel ATM- and KAP-1 dependent pathway. *Nat. Cell Biol.* **8**, 870–876 (2006).
30. D. W. Huang, B. T. Sherman, R. A. Lempicki, Systematic and integrative analysis of large gene lists using DAVID bioinformatics resources. *Nat. Protoc.* **4**, 44–57 (2009).
31. D. Schwartz, S. P. Gygi, An iterative statistical approach to the identification of protein phosphorylation motifs from large-scale data sets. *Nat. Biotechnol.* **23**, 1391–1398 (2005).
32. S. V. Kozlov, M. E. Graham, C. Peng, P. Chen, P. J. Robinson, M. F. Lavin, Involvement of novel autophosphorylation sites in ATM activation. *EMBO J.* **25**, 3504–3514 (2006).
33. M. Gatei, D. Young, K. M. Cerosaletti, A. Desai-Mehta, K. Spring, S. Kozlov, M. F. Lavin, R. A. Gatti, P. Concannon, K. Khanna, ATM-dependent phosphorylation of nibrin in response to radiation exposure. *Nat. Genet.* **25**, 115–119 (2000).
34. R. Lindling, L. J. Jensen, G. J. Ostheimer, M. A. van Vugt, C. Jørgensen, I. M. Miron, F. Diella, K. Colwill, L. Taylor, K. Elder, P. Metalnikov, V. Nguyen, A. Pasculescu, J. Jin, J. G. Park, L. D. Samson, J. R. Woodgett, R. B. Russell, P. Bork, M. B. Yaffe, T. Pawson, Systematic discovery of in vivo phosphorylation networks. *Cell* **129**, 1415–1426 (2007).
35. S. T. Kim, B. Xu, M. B. Kastan, Involvement of the cohesin protein, Smc1, in Atm-dependent and independent responses to DNA damage. *Genes Dev.* **16**, 560–570 (2002).
36. H. Luo, Y. Li, J. J. Mu, J. Zhang, T. Tonaka, Y. Hamamori, S. Y. Jung, Y. Wang, J. Qin, Regulation of intra-S phase checkpoint by ionizing radiation (IR)-dependent and IR-independent phosphorylation of SMC₃. *J. Biol. Chem.* **283**, 19176–19183 (2008).
37. P. Jowsey, N. A. Morrice, C. J. Hastie, H. McLauchlan, R. Toth, J. Rouse, Characterisation of the sites of DNA damage-induced 53BP1 phosphorylation catalysed by ATM and ATR. *DNA Repair* **6**, 1536–1544 (2007).
38. H. Lee, H. J. Kwak, I. T. Cho, S. H. Park, C. H. Lee, S1219 residue of 53BP1 is phosphorylated by ATM kinase upon DNA damage and required for proper execution of DNA damage response. *Biochem. Biophys. Res. Commun.* **378**, 32–36 (2009).
39. Y. Pereg, S. Lam, A. Teunisse, S. Biton, E. Meulmeester, L. Mittelman, G. Buscemi, K. Okamoto, Y. Taya, Y. Shiloh, A. G. Jochemsen, Differential roles of ATM- and Chk2-mediated phosphorylations of Hdmx in response to DNA damage. *Mol. Cell. Biol.* **26**, 6819–6831 (2006).
40. F. Diella, C. M. Gould, C. Chica, A. Via, T. J. Gibson, Phospho.ELM: A database of phosphorylation sites—update 2008. *Nucleic Acids Res.* **36**, D240–D244 (2008).
41. P. V. Hornbeck, I. Chabra, J. M. Kornhauser, E. Skrzypek, B. Zhang, PhosphoSite: A bioinformatics resource dedicated to physiological protein phosphorylation. *Proteomics* **4**, 1551–1561 (2004).
42. Y. Xue, J. Ren, X. Gao, C. Jin, L. Wen, X. Yao, GPS 2.0, a tool to predict kinase-specific phosphorylation sites in hierarchy. *Mol. Cell. Proteomics* **7**, 1598–1608 (2008).
43. I. Ulitsky, A. Maron-Katz, S. Shavit, D. Sagir, C. Linhart, R. Elkon, A. Tanay, R. Sharan, Y. Shiloh, R. Shamir, Expander: From expression microarrays to networks and functions. *Nat. Protoc.* **5**, 303–322 (2010).
44. R. Shamir, A. Maron-Katz, A. Tanay, C. Linhart, I. Steinfeld, R. Sharan, Y. Shiloh, R. Elkon, EXPANDER—an integrative program suite for microarray data analysis. *BMC Bioinformatics* **6**, 232 (2005).
45. L. J. Jensen, M. Kuhn, M. Stark, S. Chaffron, C. Creevey, J. Muller, T. Doerks, P. Julien, A. Roth, M. Simonovic, P. Bork, C. von Mering, STRING 8—a global view on proteins and their functional interactions in 630 organisms. *Nucleic Acids Res.* **37**, D412–D416 (2009).
46. P. Shannon, A. Markiel, O. Ozier, N. S. Baliga, J. T. Wang, D. Ramage, N. Amin, B. Schwikowski, T. Ideker, Cytoscape: A software environment for integrated models of biomolecular interaction networks. *Genome Res.* **13**, 2498–2504 (2003).

47. A. Ruepp, B. Brauner, I. Dunger-Kaltenbach, G. Frishman, C. Montrone, M. Stransky, B. Waegele, T. Schmidt, O. N. Doudieu, V. Stümpflen, H. W. Mewes, CORUM: The comprehensive resource of mammalian protein complexes. *Nucleic Acids Res.* **36**, D646–D650 (2008).
48. A. V. Antonov, S. Dietmann, I. Rodchenkov, H. W. Mewes, PPI spider: A tool for the interpretation of proteomics data in the context of protein–protein interaction networks. *Proteomics* **9**, 2740–2749 (2009).
49. G. Scardoni, M. Petterlini, C. Laudanna, Analyzing biological network parameters with CentiScaPe. *Bioinformatics* **25**, 2857–2859 (2009).
50. A. L. Barabási, R. Albert, Emergence of scaling in random networks. *Science* **286**, 509–512 (1999).
51. E. Pieroni, S. de la Fuente van Bentem, G. Mancosu, E. Capobianco, H. Hirt, A. de la Fuente, Protein networking: Insights into global functional organization of proteomes. *Proteomics* **8**, 799–816 (2008).
52. S. H. Yook, Z. N. Oltvai, A. L. Barabási, Functional and topological characterization of protein interaction networks. *Proteomics* **4**, 928–942 (2004).
53. G. Kar, A. Gursoy, O. Keskin, Human cancer protein-protein interaction network: A structural perspective. *PLoS Comput. Biol.* **5**, e1000601 (2009).
54. S. Banin, L. Moyal, S. Shieh, Y. Taya, C. W. Anderson, L. Chessa, N. I. Smorodinsky, C. Prives, Y. Reiss, Y. Shiloh, Y. Ziv, Enhanced phosphorylation of p53 by ATM in response to DNA damage. *Science* **281**, 1674–1677 (1998).
55. C. E. Canman, D. S. Lim, K. A. Cimprich, Y. Taya, K. Tamai, K. Sakaguchi, E. Appella, M. B. Kastan, J. D. Siliciano, Activation of the ATM kinase by ionizing radiation and phosphorylation of p53. *Science* **281**, 1677–1679 (1998).
56. R. V. Puspapati, R. J. Rounbehler, S. Hong, J. T. Powers, M. Yan, K. Kiguchi, M. J. McArthur, P. K. Wong, D. G. Johnson, ATM promotes apoptosis and suppresses tumorigenesis in response to *Myc*. *Proc. Natl. Acad. Sci. U.S.A.* **103**, 1446–1451 (2006).
57. K. H. Maclean, M. B. Kastan, J. L. Cleveland, *Atm* deficiency affects both apoptosis and proliferation to augment *Myc*-induced lymphomagenesis. *Mol. Cancer Res.* **5**, 705–711 (2007).
58. J. H. Park, E. J. Park, H. S. Lee, S. J. Kim, S. K. Hur, A. N. Imbalzano, J. Kwon, Mammalian SWI/SNF complexes facilitate DNA double-strand break repair by promoting γ -H2AX induction. *EMBO J.* **25**, 3986–3997 (2006).
59. S. Maere, K. Heymans, M. Kuiper, *BINGO*: A Cytoscape plugin to assess overrepresentation of Gene Ontology categories in Biological Networks. *Bioinformatics* **21**, 3448–3449 (2005).
60. L. Bozhenok, P. A. Wade, P. Varga-Weisz, WSTF-ISWI chromatin remodeling complex targets heterochromatin replication foci. *EMBO J.* **21**, 2231–2241 (2002).
61. J. P. Quivy, A. Gerard, A. J. Cook, D. Roche, G. Almouzni, The HP1–p150/CAF-1 interaction is required for pericentric heterochromatin replication and S-phase progression in mouse cells. *Nat. Struct. Mol. Biol.* **15**, 972–979 (2008).
62. S. Briers, C. Crawford, W. A. Bickmore, H. G. Sutherland, KRAB zinc-finger proteins localise to novel KAP1-containing foci that are adjacent to PML nuclear bodies. *J. Cell Sci.* **122**, 937–946 (2009).
63. R. A. Poot, L. Bozhenok, D. L. van den Berg, S. Steffensen, F. Ferreira, N. Grimaldi, N. Gilbert, J. Ferreira, P. D. Varga-Weisz, The Williams syndrome transcription factor interacts with PCNA to target chromatin remodelling by ISWI to replication foci. *Nat. Cell Biol.* **6**, 1236–1244 (2004).
64. A. Gérard, S. Koundrioukoff, V. Ramillon, J. C. Sergère, N. Mailand, J. P. Quivy, G. Almouzni, The replication kinase Cdc7-Dbf4 promotes the interaction of the p150 subunit of chromatin assembly factor 1 with proliferating cell nuclear antigen. *EMBO Rep.* **7**, 817–823 (2006).
65. J. G. Moggs, P. Grandi, J. P. Quivy, Z. O. Jonsson, U. Hubscher, P. B. Becker, G. Almouzni, A CAF-1–PCNA-mediated chromatin assembly pathway triggered by sensing DNA damage. *Mol. Cell Biol.* **20**, 1206–1218 (2000).
66. T. Rolef Ben-Shahar, A. G. Castillo, M. J. Osborne, K. L. Borden, J. Kornblatt, A. Verreault, Two fundamentally distinct PCNA interaction peptides contribute to chromatin assembly factor 1 function. *Mol. Cell Biol.* **29**, 6353–6365 (2009).
67. A. T. Noon, A. Shibata, N. Rief, M. Löbrich, G. S. Stewart, P. A. Jeggo, A. A. Goodarzi, 53BP1-dependent robust localized KAP-1 phosphorylation is essential for heterochromatin DNA double-strand break repair. *Nat. Cell Biol.* **12**, 177–184 (2010).
68. A. A. Goodarzi, A. T. Noon, D. Deckbar, Y. Ziv, Y. Shiloh, M. Löbrich, P. A. Jeggo, ATM signaling facilitates repair of DNA double-strand breaks associated with heterochromatin. *Mol. Cell* **31**, 167–177 (2008).
69. A. Xiao, H. Li, D. Shechter, S. H. Ahn, L. A. Fabrizio, H. Erdjument-Bromage, S. Ishibe-Murakami, B. Wang, P. Tempst, K. Hofmann, D. J. Patel, S. J. Elledge, C. D. Allis, WSTF regulates the H2A.X DNA damage response via a novel tyrosine kinase activity. *Nature* **457**, 57–62 (2009).
70. I. Hickson, Y. Zhao, C. J. Richardson, S. J. Green, N. M. Martin, A. I. Orr, P. M. Reaper, S. P. Jackson, N. J. Curtin, G. C. Smith, Identification and characterization of a novel and specific inhibitor of the ataxia-telangiectasia mutated kinase ATM. *Cancer Res.* **64**, 9152–9159 (2004).
71. J. S. White, S. Choi, C. J. Bakkenist, Irreversible chromosome damage accumulates rapidly in the absence of ATM kinase activity. *Cell Cycle* **7**, 1277–1284 (2008).
72. Y. Sun, Y. Xu, K. Roy, B. D. Price, DNA damage-induced acetylation of lysine 3016 of ATM activates ATM kinase activity. *Mol. Cell Biol.* **27**, 8502–8509 (2007).
73. Y. Ziv, A. Bar-Shira, I. Pecker, P. Russell, T. J. Jorgensen, I. Tsarfati, Y. Shiloh, Recombinant ATM protein complements the cellular A-T phenotype. *Oncogene* **15**, 159–167 (1997).
74. Y. Andegeko, L. Moyal, L. Mittelman, I. Tsarfati, Y. Shiloh, G. Rotman, Nuclear retention of ATM at sites of DNA double strand breaks. *J. Biol. Chem.* **276**, 38224–38230 (2001).
75. S. So, A. J. Davis, D. J. Chen, Autophosphorylation at serine 1981 stabilizes ATM at DNA damage sites. *J. Cell Biol.* **187**, 977–990 (2009).
76. Y. B. Wu, J. Dai, X. L. Yang, S. J. Li, S. L. Zhao, Q. H. Sheng, J. S. Tang, G. Y. Zheng, Y. X. Li, J. R. Wu, R. Zeng, Concurrent quantification of proteome and phosphoproteome to reveal system-wide association of protein phosphorylation and gene expression. *Mol. Cell Proteomics* **8**, 2809–2826 (2009).
77. F. Wu, P. Wang, J. Zhang, L. C. Young, R. Lai, L. Li, Studies of phosphoproteomic changes induced by nucleophosmin-anaplastic lymphoma kinase (ALK) highlight deregulation of tumor necrosis factor (TNF)/Fas/TNF-related apoptosis-induced ligand signaling pathway in ALK-positive anaplastic large cell lymphoma. *Mol. Cell Proteomics* **9**, 1616–1632 (2010).
78. P. C. Bonnette, B. S. Robinson, J. C. Silva, M. P. Stokes, A. D. Brosius, A. Baumann, L. Buckbinder, Phosphoproteomic characterization of PYK2 signaling pathways involved in osteogenesis. *J. Proteomics* **73**, 1306–1320 (2010).
79. H. Kosako, N. Yamaguchi, C. Aranami, M. Ushiyama, S. Kose, N. Imamoto, H. Taniguchi, E. Nishida, S. Hattori, Phosphoproteomics reveals new ERK MAP kinase targets and links ERK to nucleoporin-mediated nuclear transport. *Nat. Struct. Mol. Biol.* **16**, 1026–1035 (2009).
80. V. Mayya, D. H. Lundgren, S. I. Hwang, K. Rezaul, L. Wu, J. K. Eng, V. Rodionov, D. K. Han, Quantitative phosphoproteomic analysis of T cell receptor signaling reveals system-wide modulation of protein-protein interactions. *Sci. Signal.* **2**, ra46 (2009).
81. R. M. Larive, S. Urbach, J. Poncet, P. Jouin, G. Mascre, A. Sahuquet, P. H. Mangeat, P. J. Coopman, N. Bettache, Phosphoproteomic analysis of Syk kinase signaling in human cancer cells reveals its role in cell–cell adhesion. *Oncogene* **28**, 2337–2347 (2009).
82. E. Riballo, M. Kühne, N. Rief, A. Doherty, G. C. Smith, M. J. Recio, C. Reis, K. Dahm, A. Fricke, A. Krempler, A. R. Parker, S. P. Jackson, A. Gennery, P. A. Jeggo, M. Löbrich, A pathway of double-strand break rejoining dependent upon ATM, Artemis, and proteins locating to γ -H2AX foci. *Mol. Cell Biol.* **16**, 715–724 (2004).
83. H. C. Reinhardt, M. B. Yaffe, Kinases that control the cell cycle in response to DNA damage: Chk1, Chk2, and MK2. *Curr. Opin. Cell Biol.* **21**, 245–255 (2009).
84. F. Meggio, L. A. Pinna, One-thousand-and-one substrates of protein kinase CK2? *FASEB J.* **17**, 349–368 (2003).
85. N. Ayoub, A. D. Jeyasekharan, J. A. Bernal, A. R. Venkiteswaran, HP1- β mobilization promotes chromatin changes that initiate the DNA damage response. *Nature* **453**, 682–686 (2008).
86. F. Melander, S. Bekker-Jensen, J. Falck, J. Bartek, N. Mailand, J. Lukas, Phosphorylation of SDT repeats in the MDC1 N terminus triggers retention of NBS1 at the DNA damage-modified chromatin. *J. Cell Biol.* **181**, 213–226 (2008).
87. C. Spycher, E. S. Miller, K. Townsend, L. Pavic, N. A. Morrice, P. Janscak, G. S. Stewart, M. Stucki, Constitutive phosphorylation of MDC1 physically links the MRE11–RAD50–NBS1 complex to damaged chromatin. *J. Cell Biol.* **181**, 227–240 (2008).
88. A. Ali, J. Zhang, S. Bao, I. Liu, D. Otterness, N. M. Dean, R. T. Abraham, X. F. Wang, Requirement of protein phosphatase 5 in DNA-damage-induced ATM activation. *Genes Dev.* **18**, 249–254 (2004).
89. W. Yong, S. Bao, H. Chen, D. Li, E. R. Sanchez, W. Shou, Mice lacking protein phosphatase 5 are defective in ataxia telangiectasia mutated (ATM)-mediated cell cycle arrest. *J. Biol. Chem.* **282**, 14690–14694 (2007).
90. P. Petersen, D. M. Chou, Z. You, T. Hunter, J. C. Walter, G. Walter, Protein phosphatase 2A antagonizes ATM and ATR in a Cdk2- and Cdc7-independent DNA damage checkpoint. *Mol. Cell Biol.* **26**, 1997–2011 (2006).
91. D. Chowdhury, M. C. Keogh, H. Ishii, C. L. Peterson, S. Buratowski, J. Lieberman, γ -H2AX dephosphorylation by protein phosphatase 2A facilitates DNA double-strand break repair. *Mol. Cell* **20**, 801–809 (2005).
92. A. A. Goodarzi, J. C. Jonnalagadda, P. Douglas, D. Young, R. Ye, G. B. Moorhead, S. P. Lees-Miller, K. K. Khanna, Autophosphorylation of ataxia-telangiectasia mutated is regulated by protein phosphatase 2A. *EMBO J.* **23**, 4451–4461 (2004).
93. S. Shreeram, O. N. Demidov, W. K. Hee, H. Yamaguchi, N. Onishi, C. Kek, O. N. Timofeev, C. Dudgeon, A. J. Fornace, C. W. Anderson, Y. Minami, E. Appella, D. V. Bulavin, Wip1 phosphatase modulates ATM-dependent signaling pathways. *Mol. Cell* **23**, 757–764 (2006).
94. H. Yamaguchi, S. R. Durell, D. K. Chatterjee, C. W. Anderson, E. Appella, The Wip1 phosphatase PPM1D dephosphorylates SQ/TQ motifs in checkpoint substrates phosphorylated by PI3K-like kinases. *Biochemistry* **46**, 12594–12603 (2007).
95. X. Lu, T. A. Nguyen, L. A. Donehower, Reversal of the ATM/ATR-mediated DNA damage response by the oncogenic phosphatase PPM1D. *Cell Cycle* **4**, 1060–1064 (2005).

96. C. Y. Guo, D. L. Brautigan, J. M. Lamer, Ionizing radiation activates nuclear protein phosphatase-1 by ATM-dependent dephosphorylation. *J. Biol. Chem.* **277**, 41756–41761 (2002).
97. X. Tang, Z. G. Hui, X. L. Cui, R. Garg, M. B. Kastan, B. Xu, A novel ATM-dependent pathway regulates protein phosphatase 1 in response to DNA damage. *Mol. Cell. Biol.* **28**, 2559–2566 (2008).
98. A. Peng, A. L. Lewellyn, W. P. Schieman, J. L. Maller, Repo-Man controls a protein phosphatase 1-dependent threshold for DNA damage checkpoint activation. *Curr. Biol.* **20**, 387–396 (2010).
99. S. Bamford, E. Dawson, S. Forbes, J. Clements, R. Pettett, A. Dogan, A. Flanagan, C. J. Teague, P. A. Futreal, M. R. Stratton, R. Wooster, The COSMIC (Catalogue of Somatic Mutations in Cancer) database and website. *Br. J. Cancer* **91**, 355–358 (2004).
100. P. T. Wan, M. J. Gamett, S. M. Roe, S. Lee, D. Niculescu-Duvaz, V. M. Good, C. M. Jones, C. J. Marshall, C. J. Springer, D. Barford, R. Marais, Cancer Genome Project, Mechanism of activation of the RAF-ERK signaling pathway by oncogenic mutations of B-RAF. *Cell* **116**, 855–867 (2004).
101. M. E. Olsten, D. W. Litchfield, Order or chaos? An evaluation of the regulation of protein kinase CK2. *Biochem. Cell Biol.* **82**, 681–693 (2004).
102. N. A. St-Denis, D. W. Litchfield, Protein kinase CK2 in health and disease: From birth to death: The role of protein kinase CK2 in the regulation of cell proliferation and survival. *Cell. Mol. Life Sci.* **66**, 1817–1829 (2009).
103. R. D. Paulsen, D. V. Soni, R. Wollman, A. T. Hahn, M. C. Yee, A. Guan, J. A. Hesley, S. C. Miller, E. F. Cromwell, D. E. Solow-Cordero, T. Meyer, K. A. Cimprich, A genome-wide siRNA screen reveals diverse cellular processes and pathways that mediate genome stability. *Mol. Cell* **35**, 228–239 (2009).
104. M. Salton, Y. Lerenthal, S. Y. Wang, D. J. Chen, Y. Shiloh, Involvement of Matrin 3 and SFPQ/NONO in the DNA damage response. *Cell Cycle* **9**, 1568–1576 (2010).
105. S. Britton, C. Froment, P. Frit, B. Monsarrat, B. Salles, P. Calsou, Cell nonhomologous end joining capacity controls SAF-A phosphorylation by DNA-PK in response to DNA double-strand breaks inducers. *Cell Cycle* **8**, 3717–3722 (2009).
106. N. Zhang, R. Kaur, S. Akhter, R. J. Legerski, Cdc5L interacts with ATR and is required for the S-phase cell-cycle checkpoint. *EMBO Rep.* **10**, 1029–1035 (2009).
107. N. Zhang, R. Kaur, X. Lu, X. Shen, L. Li, R. J. Legerski, The Pso4 mRNA splicing and DNA repair complex interacts with WRN for processing of DNA interstrand cross-links. *J. Biol. Chem.* **280**, 40559–40567 (2005).
108. V. Leung-Pineda, C. E. Ryan, H. Piwnicka-Worms, Phosphorylation of Chk1 by ATR is antagonized by a Chk1-regulated protein phosphatase 2A circuit. *Mol. Cell. Biol.* **26**, 7529–7538 (2006).
109. P. M. DeHé, M. Pamblanco, P. Luciano, R. Lebrun, D. Moinier, R. Sendra, A. Verreault, V. Tordera, V. Géli, Histone H3 lysine 4 mono-methylation does not require ubiquitination of histone H2B. *J. Mol. Biol.* **353**, 477–484 (2005).
110. H. Fujimoto, N. Onishi, N. Kato, M. Takekawa, X. Z. Xu, A. Kosugi, T. Kondo, M. Imamura, I. Oishi, A. Yoda, Y. Minami, Regulation of the antioncogenic Chk2 kinase by the oncogenic Wip1 phosphatase. *Cell Death Differ.* **13**, 1170–1180 (2006).
111. A. Yoda, X. Z. Xu, N. Onishi, K. Toyoshima, H. Fujimoto, N. Kato, I. Oishi, T. Kondo, Y. Minami, Intrinsic kinase activity and SQ/TQ domain of Chk2 kinase as well as N-terminal domain of Wip1 phosphatase are required for regulation of Chk2 by Wip1. *J. Biol. Chem.* **281**, 24847–24862 (2006).
112. X. Lu, O. Ma, T. A. Nguyen, S. N. Jones, M. Oren, L. A. Donehower, The Wip1 phosphatase acts as a gatekeeper in the p53-Mdm2 autoregulatory loop. *Cancer Cell* **12**, 342–354 (2007).
113. X. Zhang, L. Lin, H. Guo, J. Yang, S. N. Jones, A. Jochemsen, X. Lu, Phosphorylation and degradation of MdmX is inhibited by Wip1 phosphatase in the DNA damage response. *Cancer Res.* **69**, 7960–7968 (2009).
114. L. Macurek, A. Lindqvist, O. Voets, J. Kool, H. R. Vos, R. H. Medema, Wip1 phosphatase is associated with chromatin and dephosphorylates γ H2AX to promote checkpoint inhibition. *Oncogene* **29**, 2281–2291 (2010).
115. S. H. Moon, L. Lin, X. Zhang, T. A. Nguyen, Y. Darlington, A. S. Waldman, X. Lu, L. A. Donehower, Wild-type p53-induced phosphatase 1 dephosphorylates histone variant γ -H2AX and suppresses DNA double strand break repair. *J. Biol. Chem.* **285**, 12935–12947 (2010).
116. E. Batchelor, C. S. Mock, I. Bhan, A. Loewer, G. Lahav, Recurrent initiation: A mechanism for triggering p53 pulses in response to DNA damage. *Mol. Cell* **30**, 277–289 (2008).
117. R. Heinrich, B. G. Neel, T. A. Rapoport, Mathematical models of protein kinase signal transduction. *Mol. Cell* **9**, 957–970 (2002).
118. J. J. Homberg, F. J. Bruggeman, B. Binder, C. R. Geest, A. J. de Vaate, J. Lankelma, R. Heinrich, H. V. Westerhoff, Principles behind the multifarious control of signal transduction. ERK phosphorylation and kinase/phosphatase control. *FEBS J.* **272**, 244–258 (2005).
119. Y. Sun, Y. Xu, K. Roy, B. D. Price, DNA damage-induced acetylation of lysine 3016 of ATM activates ATM kinase activity. *Mol. Cell. Biol.* **27**, 8502–8509 (2007).
120. B. Tian, Q. Yang, Z. Mao, Phosphorylation of ATM by Cdk5 mediates DNA damage signalling and regulates neuronal death. *Nat. Cell Biol.* **11**, 211–218 (2009).
121. M. Pellegrini, A. Celeste, S. Difilippantonio, R. Guo, W. Wang, L. Feigenbaum, A. Nussenzweig, Autophosphorylation at serine 1987 is dispensable for murine Atm activation in vivo. *Nature* **443**, 222–225 (2006).
122. J. A. Daniel, M. Pellegrini, J. H. Lee, T. T. Paull, L. Feigenbaum, A. Nussenzweig, Multiple autophosphorylation sites are dispensable for murine ATM activation in vivo. *J. Cell Biol.* **183**, 777–783 (2008).
123. M. V. Bennetzen, D. H. Larsen, J. Bunkenborg, J. Bartek, J. Lukas, J. S. Andersen, Site-specific phosphorylation dynamics of the nuclear proteome during the DNA damage response. *Mol. Cell. Proteomics* **9**, 1314–1323 (2010).
124. J. J. Leahy, B. T. Golding, R. J. Griffin, I. R. Hardcastle, C. Richardson, L. Rigoreau, G. C. Smith, Identification of a highly potent and selective DNA-dependent protein kinase (DNA-PK) inhibitor (NU7441) by screening of chromonone libraries. *Bioorg. Med. Chem. Lett.* **14**, 6083–6087 (2004).
125. M. W. Pinkse, P. M. Uitto, M. J. Hilhorst, B. Ooms, A. J. Heck, Selective isolation at the femtomole level of phosphopeptides from proteolytic digests using 2D-nanoLC-ESI-MS/MS and titanium oxide precolumns. *Anal. Chem.* **76**, 3935–3943 (2004).
126. J. R. Yates III, J. K. Eng, A. L. McCormack, D. Schieltz, Method to correlate tandem mass spectra of modified peptides to amino acid sequences in the protein database. *Anal. Chem.* **67**, 1426–1436 (1995).
127. A. Keller, J. Eng, N. Zhang, X. J. Li, R. Aebersold, A uniform proteomics MS/MS analysis platform utilizing open XML file formats. *Mol. Syst. Biol.* **1**, 2005.0017 (2005).
128. S. A. Beausoleil, J. Villen, S. A. Gerber, J. Rush, S. P. Gygi, A probability-based approach for high-throughput protein phosphorylation analysis and site localization. *Nat. Biotechnol.* **24**, 1285–1292 (2006).
129. L. N. Mueller, O. Rinner, A. Schmidt, S. Letarte, B. Bodenmiller, M. Y. Brusniak, O. Vitek, R. Aebersold, M. Muller, *SuperHim*—a novel tool for high resolution LC-MS-based peptide/protein profiling. *Proteomics* **7**, 3470–3480 (2007).
130. M. Y. Brusniak, B. Bodenmiller, D. Campbell, K. Cooke, J. Eddes, A. Garbutt, H. Lau, S. Letarte, L. N. Mueller, V. Sharma, O. Vitek, N. Zhang, R. Aebersold, J. D. Watts, Corra: Computational framework and tools for LC-MS discovery and targeted mass spectrometry-based proteomics. *BMC Bioinformatics* **9**, 542 (2008).
131. N. Uematsu, E. Weterings, K. Yano, K. Morotomi-Yano, B. Jakob, G. Taucher-Scholz, P. O. Mari, D. C. van Gent, B. P. Chen, D. J. Chen, Autophosphorylation of DNA-PKCS regulates its dynamics at DNA double-strand breaks. *J. Cell Biol.* **177**, 219–229 (2007).
132. **Acknowledgments:** We thank M. Kastan, K. Yokomori, and M. Lavin for reagents and B. Bodenmiller for important advice. **Funding:** This work was supported by research grants from the European Community's Seventh Framework Programme (HEALTH-F4-2009-223575, the TRIREME Project), the A-T Medical Research Foundation, and the Israel Cancer Research Fund to Y.S., and the NIH (CA050519 and CA13499) to D.J.C. Y.S. is a Research Professor of the Israel Cancer Research Fund. **Author contributions:** A.B., A.S., and S.-Y.W. carried out experimental work and took part in the experimental design; Y.Z., R.E., D.J.C., R.A., and Y.S. contributed to the experimental design; A.B. carried out the computational work with help and advice from A.S. and R.E.; A.B. and Y.S. wrote the manuscript, with further contributions from Y.Z., R.E., D.J.C., and R.A. **Competing interests:** The authors declare that they have no competing interests.

Submitted 26 March 2010

Accepted 15 November 2010

Final Publication 7 December 2010

10.1126/scisignal.2001034

Citation: A. Schimidt, Y. Ziv, R. Elkon, S.-Y. Wang, D. J. Chen, R. Aebersold, Y. Shiloh, ATM-dependent and -independent dynamics of the nuclear phosphoproteome after DNA damage. *Sci. Signal.* **3**, rs3 (2010).